Cement and Concrete Research 156 (2022) 106784

Contents lists available at ScienceDirect

Cement and Concrete Research

journal homepage: www.elsevier.com/locate/cemconres

A comprehensive review of C-S-H empirical and computational models, their applications, and practical aspects

Eduardo Duque-Redondo [a,b,*], Patrick A. Bonnaud [c], Hegoi Manzano [d]

[a] School of Engineering, Newcastle University, NE1 7RU Newcastle upon Tyne, UK
[b] Physical Chemistry Department, University of the Basque Country UPV/EHU, Aptdo. 664, 48080 Bilbao, Spain
[c] Research Organization for Information Science and Technology, Department of Computational Science and Technology, 1-18-16 Hamamatsucho, Minato 105-0013, Tokyo, Japan
[d] Fisika Saila, University of the Basque Country UPV/EHU, Aptdo. 664, 48080 Bilbao, Spain

ARTICLE INFO

Keywords:
Calcium silicate hydrate
Molecular models
Molecular simulation
Atomic structure
Nanostructure

ABSTRACT

The C-S-H gel is an elusive material. Its variable composition and disordered nature complicate a complete characterization of its atomic structure, and the elaboration of models is key to understanding it. This work aims to review those proposed models, dividing them into empirical and computational models. After a brief description of related crystalline calcium silicate hydrates, empirical C-S-H models based on interpretation of experimental data are presented. Then, we focus on the historic development of atomistic models to study the C-S-H, until the current state of the art. We describe current computational C-S-H models built from the empirical models and computer simulations. We review common applications of these computational models: the aluminum incorporation, the elastic and mechanical properties, the diffusion of water and ions in nanopores, and C-S-H/organic composites. Finally, we discuss some practical aspects of the computational models and their interpretation, as well as possible future directions.

1. Introduction

Ordinary Portland cement is arguably the most consumed man-made material worldwide. As such, there is a vast amount of empirical information on the material and how to control its workability, durability, or strength [1–4]. Thus, it is surprising how much remains unknown from a fundamental point of view, especially if we compare cement to other construction materials like steel, or commonly used materials like silicon. The lack of knowledge is particularly notable at the nanoscale, where the complex, multicomponent, porous, and disordered structure of cement hydrates complicates the experimental characterization of the material. The dominant phase at that scale is the Calcium Silicate Hydrate (C-S-H) gel, an X-ray amorphous product with variable chemical composition and structure. The C-S-H gel is the glue that agglomerates other crystalline hydration products and aggregates, giving cohesion to the material, and is mainly responsible for cement's mechanical properties and durability.

Plausible strategies to increase cement's performance and reduce its environmental footprint include a fine control of the C-S-H gel structure, properties, or its precipitation kinetics. Traditionally an empirical trial-error approach has been used for those ends [5–7], yet most recent studies benefit from the existing information at the atomic scale to design bottom-up synthetic approaches [8–12]. To extract valuable information from the available vast amount of experimental data, the observations must be condensed into comprehensive models consistent with as much as possible data. Many different models have been proposed so far to rationalize the experimental findings and understand the atomic structure of the C-S-H gel. Ideally, those models should be able not only to explain experimental observations but also be predictive, and help to devise a material with tailored properties.

In this paper, we aim to describe briefly most of the models for the C-S-H gel structure proposed in the literature. We divided them into two categories: empirical models and computational models. The first group includes suggestions made on the basis of experimental facts collected over six decades. These empirical models aimed to describe the C-S-H gel structure by comparison with related crystals like portlandite or the tobermorite family and often included stoichiometric formulas. The second group covers the more detailed atomic-scale models developed in the last decade using computational simulations. These models try to define the C-S-H gel structure with the greatest possible detail,

* Corresponding author at: School of Engineering, Newcastle University, NE1 7RU Newcastle upon Tyne, UK
E-mail addresses: eduardo.duque@ehu.eus (E. Duque-Redondo), bonnaud@rist.or.jp (P.A. Bonnaud), hegoi.manzano@ehu.eus (H. Manzano).

https://doi.org/10.1016/j.cemconres.2022.106784
Received 31 May 2021; Received in revised form 15 March 2022; Accepted 17 March 2022
Available online 7 April 2022

specifying the coordinates (spatial position) of every atom in the material. Nowadays, one group cannot be understood without the other. On the one hand, empirical models are "just" schematic representations that compile experimental information, yet they set the structural conditions and stoichiometric rules that should be fulfilled in the computational model construction. On the other hand, atomic-scale computational models based on the empirical rules go beyond a mere description and can be used to compute actual C-S-H properties, to help in the interpretation of experimental data, or even contribute with new information inaccessible to experiments. Examples of how C-S-H modeling is used to get insights into and deep understanding are provided in Section 5.

The remaining paper is organized as follows: first, we will introduce briefly the crystalline phases commonly used as starting points for C-S-H model construction. Second, we will survey the empirical models proposed over the years to describe the C-S-H gel and the recent computational models. Due to the increasing interest in atomistic simulation, we will review the main applications of computational models such as the study of the aluminum incorporation into the C-S-H gel, its elasticity, and mechanical properties, the nanoconfined water within the C-S-H gel layers, the ion diffusivity, and the formation of C-S-H/organic hybrid composites. We skipped other topics of great interest like C-S-H nucleation and growth or C-S-H carbonation because much less literature is available yet. Finally, we will discuss practical aspects and our perspective on future directions.

2. Crystalline structures related to C-S-H

The C-S-H gel is an X-ray amorphous material and does not present long-range order like a crystal. However, it is possible to find short-range order at the atomic scale. NMR, IR-spectroscopy, synchrotron X-ray diffraction, and SANS experiments among others [13–19], reveal the C-S-H gel similarities with crystalline calcium silicate hydrates [20] like wollastonite, jennite, hillebrandite, and specially tobermorite. There is a general consensus that the C-S-H structure is similar to the tobermorite family members [21], with a considerable number of structural defects and variable stoichiometry even at low Ca/Si ratios [22].

The tobermorite supergroup is the classification of a family of minerals with a layered structure similar to clays. The family includes various members of the tobermorite group plus related minerals like plombièrite, clinotobermorite, and riversideite. They differ in the basal spacing (related to the hydration degree) and cell symmetry. Plombièrite, clinotobermorite, and riversideite exhibit basal spacing of 1.4, 1.1, and 0.9 nm, respectively, and have Ca/Si ratios of 5/6, with compositions: $Ca_5Si_6O_{16}(OH)_2{\cdot}7H_2O$, $Ca_5Si_6O_{17}{\cdot}5H_2O$ and $Ca_5Si_6O_{16}(OH)_2$ respectively. The basal spacing in the tobermorite group is ~1.1 nm and the Ca/Si ratio is not always 5/6. The general formula of the tobermorite group is $Ca_{4+x}(Si_6)O_{15+2x}(OH)_{2-2x}{\cdot}5H_2O$, with $0 \leq x \leq 1$. Thus, the endmember compositions correspond to tobermorite $Ca_5Si_6O_{17}{\cdot}5H_2O$ ($x = 1$) and to kenotobermorite, $Ca_4Si_6O_{15}(OH)_2{\cdot}5H_2O$ ($x = 0$). In general, the tobermorite supergroup members are made of layers, each of them consisting of a central calcium oxide sheet, sharing oxygens with *dreierketten* or wollastonite-like silicate chains at each side of it. These chains run parallel to the b crystallographic axis, and *dreierketten* denotes an arrangement that repeats every three silicate units. In tobermorite, two consecutive units, denoted as pairing sites, are linked to the central calcium oxide layer sharing two out of their four oxygen atoms. The third silicate unit, called bridging site, is oriented towards the interlaminar space for steric reasons [23]. The Ca atoms in the central calcium oxide sheet follow a zig-zag arrangement, with poorly symmetric 7-fold coordination to oxygen atoms [24]. This structural module, characterized by a central calcium oxide sheet with 7-fold coordination sandwiched between *dreierketten* or wollastonite-like chains, is known as a "complex module" [25]. In the crystal, the calcium silicate layers lie on the xy or (001) plane, while the periodicity in the z-direction comes from the stacking of layers. The interlayer space is filled by water and extra calcium ions which provide cohesion via dispersive and electrostatic interactions respectively (see Fig. 1) [26]. As mentioned before, the tobermorite supergroup comprises several polytypes: the main ones being tobermorite 0.9 nm, tobermorite 1.1 nm, and tobermorite 1.4 nm (see Fig. 1). These polytypes differ mainly in the basal spacing (the distance in the z crystallographic direction between the center of two consecutive layers), which is wider as the hydration degree increases. Thus, from tobermorite 1.4 nm, it is possible to obtain tobermorite 1.1 nm, and tobermorite 0.9 nm by heating or dehydration. Another important difference between polytypes is the interlayer cross-link in tobermorite 1.1 nm. The silicate chains from adjacent layers can be linked in the c crystallographic direction by condensation of the bridging sites, forming a double wollastonite chain with "zeolitic cavities". The protonation and Al content of silicate chains, as well as the Ca content in the cavities, define the dehydration behavior of the 1.1 nm polytype, which is sorted into normal and anomalous varieties. Thus, the presence of interlayer cross-linkages in anomalous tobermorites restrains the shrinkage during the dehydration, maintaining their characteristic basal spacing, while the absence of interlayer Si-O-Si linkages in normal tobermorites, allows the decrease of the basal spacing and the transformation of tobermorite 1.1 nm into tobermorite 0.9 nm [27,28].

Recent studies [19,29] suggested clinotobermorite as the tobermorite family member matching the best with the C-S-H gel atomic structure.The differences between clinotobermorite and tobermorite 1.1 nm are subtle, and they tend to coexist [21]. Their composition is very similar, yet the hydroxyl groups of the bridging tetrahedra are missing in clinotobermorite, resulting in the stoichiometry $Ca_5Si_6O_{17} \times 5H_2O$. Furthermore, the orientation of the top and bottom bridging tetrahedra of a given layer alternate left and right, while in tobermorite 1.1 nm they point in the same direction. This difference has been classified by naming the complex modules (see Fig. 2) as A and B for clinotobermorite and tobermorite 1.1 nm respectively.

Hamid's tobermorite must be also mentioned here [30]. It was an early attempt to resolve the crystalline structure of tobermorite 1.1 nm. The basal distance is 1.117 nm, which is shorter than the one for the normal or anomalous tobermorite 1.1 nm. The stoichiometry is $Ca_{4.5}Si_6O_{15}(OH)_3 \times 2H_2O$. In contrast to Merlino's tobermorite 1.1 nm, Hamid's model does not include interlayer cross-links between bridging silicates from adjacent layers. Like in tobermorite 0.9 nm and 1.4 nm, the silicate chains from adjacent layers are shifted in the b crystallographic direction by b/2, so the bridging sites do not face each other. The layers are also shifted in the z crystallographic axis by z/4, so they are not located in the same cleavage (see Fig. 2).

Jennite description is also included here because historically it was considered as a possible model for the C-S-H gel with high Ca/Si ratios [31]. Nowadays, the models based on jennite have lost interest. Recent experiments show that high Ca/Si ratio structures can be also formed maintaining a tobermorite-like structure, and both experimental and theoretical works indicate that tobermorite structural fingerprints match with the C-S-H [32–34]. Jennite can be found combined with tobermorite in nature or can be obtained by hydrothermal synthesis [35,36]. It has a stoichiometry $Ca_9Si_6O_{18}(OH)_6 \times 8H_2O$ and a Ca/Si ratio of 1.55. The structures of jennite and tobermorite are related, since they both have a layered structure and wollastonite-like silicate chains. However, there are two alternated calcium oxide slabs in each layer of jennite, which allows the bridging silicates to be connected to the calcium oxide layer. In addition, the higher calcium content of jennite implies that the calcium coordination polyhedral, hexagonal in this case, are completed with hydroxyl groups.

3. Empirical C-S-H gel models

In recent years there is a clear shift from empirical models to computational models, so very few additions have been done lately. Nevertheless, there are a couple of noteworthy works that should be mentioned. In this section, we will revisit the most relevant empirical models proposed to describe the C-S-H gel structure. We must mention

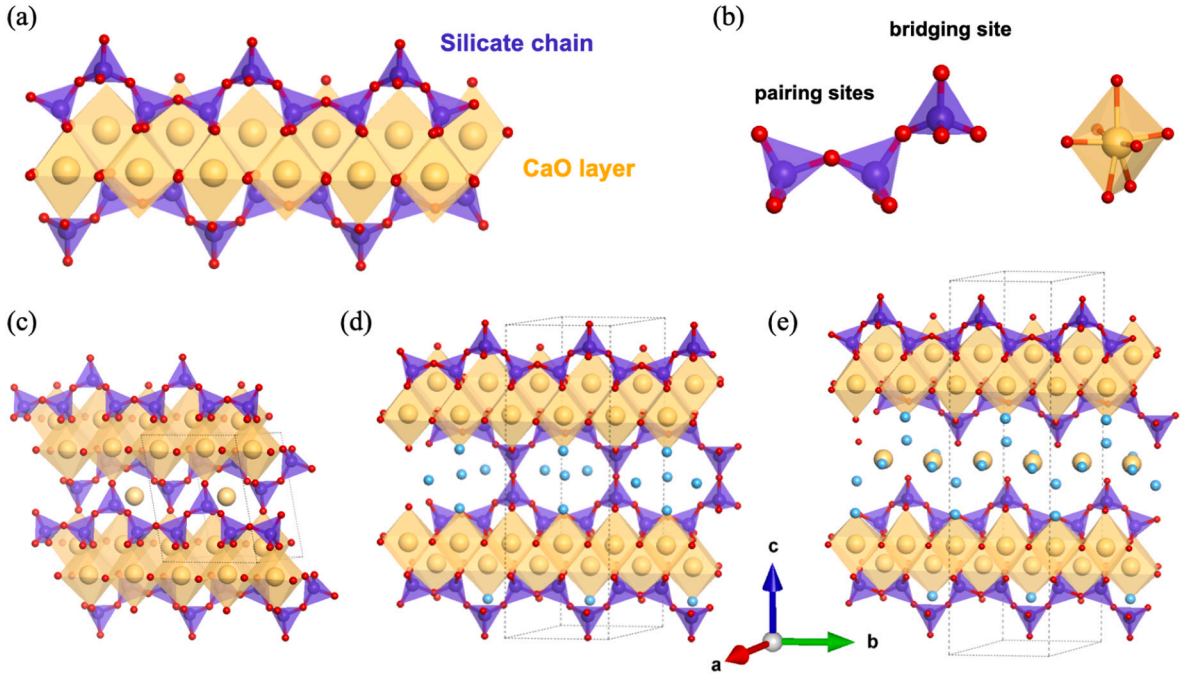

Fig. 1. (a) Detail of the calcium silicate layer, the main structural motif in calcium silicate hydrates. (b) Detail of the *dreierketten* or wollastonite-like arrangement in the silicate chains, and the 7-fold coordination of Ca. (c) Atomic representation of the structure of tobermorite 0.9 nm (d) tobermorite 1.1 nm and (e) tobermorite 1.4 nm. The prisms formed by the dashed lines represent the unit cells of the polytypes of tobermorite. To facilitate the visualization of their layered structure, the unit cells have been replicated 2 times along the b-axis in all cases and 1 along the c-axis for the tobermorite 0.9 nm. Silicate atoms are shown in purple, calcium atoms in orange, and oxygen atoms in red. The interlaminar water molecules are represented by a blue ball in the molecular center of mass, and all hydrogen atoms are omitted for a better view. (For interpretation of the references to colour in this figure legend, the reader is referred to the web version of this article.)

that there is an extensive review by Richardson in [20] discussing these models in great detail.

Layered C-S-H models were first proposed in 1952 by Bernal and coworkers based on the X-ray diffraction (XRD) patterns [37,38]. First, they suggested that two types of C-S-H were obtained from cement hydration, both of them were the result of a portlandite modification via condensation of monomeric silicate anions [37]. Their general stoichiometry was $Ca[SiO_2(OH)_2][Ca(OH)_2]_x$, with an extra amount of water. Later, other authors also proposed models based on portlandite and monomeric silicate groups. In 1969, Shpynova et al. [39] postulated a $Ca_3(SiO_4)(OH)_2$ stoichiometry, as a result of the condensation of the 4 hydroxyl groups of an orthosilicic acid molecule with portlandite. In 1986, Grudemo et al. [40] proposed again a portlandite-silicate monomer model similar to the previous ones. However, all these models were soon deprecated due to the inconsistency with the experimental distribution of silicate groups found by ^{29}Si NMR measurements [41,42], in which the chains follow the rule $3n - 1$ with n being an integer.

Also in 1952, Bernal, Jeffery, and Taylor [38] pointed for the first time to the relationship between the atomic structure of C-S-H gel and tobermorite. They analyzed by XRD the hydration product of tricalcium silicate and cement samples, concluding that "out of ten (samples) for which single crystal or oriented fiber data could be obtained, seven had one axis of 3.65 or 2 x 3.65 Å" [38], being those lengths equal to the mineral riversideite (tobermorite 0.9 nm [21]). They stressed that the marked fibrous character of the C-S-H was consistent with those minerals, yet they do not explain further details on the differences between tobermorite and the C-S-H.

A few years later, in 1956, Taylor and Howison addressed the differences in composition between tobermorite and the C-S-H, especially the high Ca/Si ratio of the latter [43]. Based on the fact that the silicate chains in tobermorite have a *dreierketten* arrangement, they postulated that a partial omission of some bridging silicate tetrahedra and their replacement by calcium ions in the interlayer spaces could increase the Ca/Si ratio of tobermorite from 0.83 up to 1.5. [43]. This is in practice the first mention of a C-S-H model based on tobermorite with finite silicate chains, and already introduced the main *motifs* that nowadays are still considered the source of C-S-H disorder.

In the early 60s, Kurczyk and Schwiete measured the Ca/Si ratio of the C-S-H formed in tricalcium and dicalcium silicates, obtaining values ranging from 1.80 to 1.92 [44,45]. Assuming a tobermorite-like C-S-H retaining its infinite silicate chains, they explained the discrepancy envisioning a C-S-H gel in which calcium cations and hydroxyl anions were located in the interlayer space of tobermorite. At the same time, Kantro, Brunauer, and Weiss suggested that the high Ca/Si ratio could be reached due to specific arrangements of sandwiched tobermorite layers between calcium hydroxide ones [46], while Fujii and Kondo considered that was due to a solid solution of tobermorite and portlandite [47]. However, all these models considered infinite silicate chains, which is not consistent with experimental observations.

In the 1980s, Stade and Wieker designed a model based on the tobermorite structure with finite silicate chains [48,49]. They proposed a dual model: one purely dimeric, and another one mixing dimeric and polymeric chains. These models assumed full protonation of the silicate chains and were limited to the compositions studied by the authors, with Ca/Si ratios below 1.25. [48,49]. Glasser et al. [50] extended the dimeric model assuming partial deprotonation of the silicate chains and adding extra Ca ions to counterbalance the charge, reaching Ca/Si ratios up to 1.4.

Based on his previous model [43], Taylor envisaged in 1986 a C-S-H gel model built by a combination of structural units of tobermorite and jennite [17,51]. According to his work, the partial deletion of some silicate bridging tetrahedra from the infinite silicate chains of tobermorite and jennite's structures results in higher Ca/Si ratios and finite silicate chains that follow the $3n - 1$ rule. In contrast to its previous model, the interlayer calcium remains unchanged since it is assumed that the deleted bridging tetrahedra have only one hydrogen and one of the new ends of the finite silicate chains is protonated, maintaining the electroneutrality of the system without adding extra Ca.

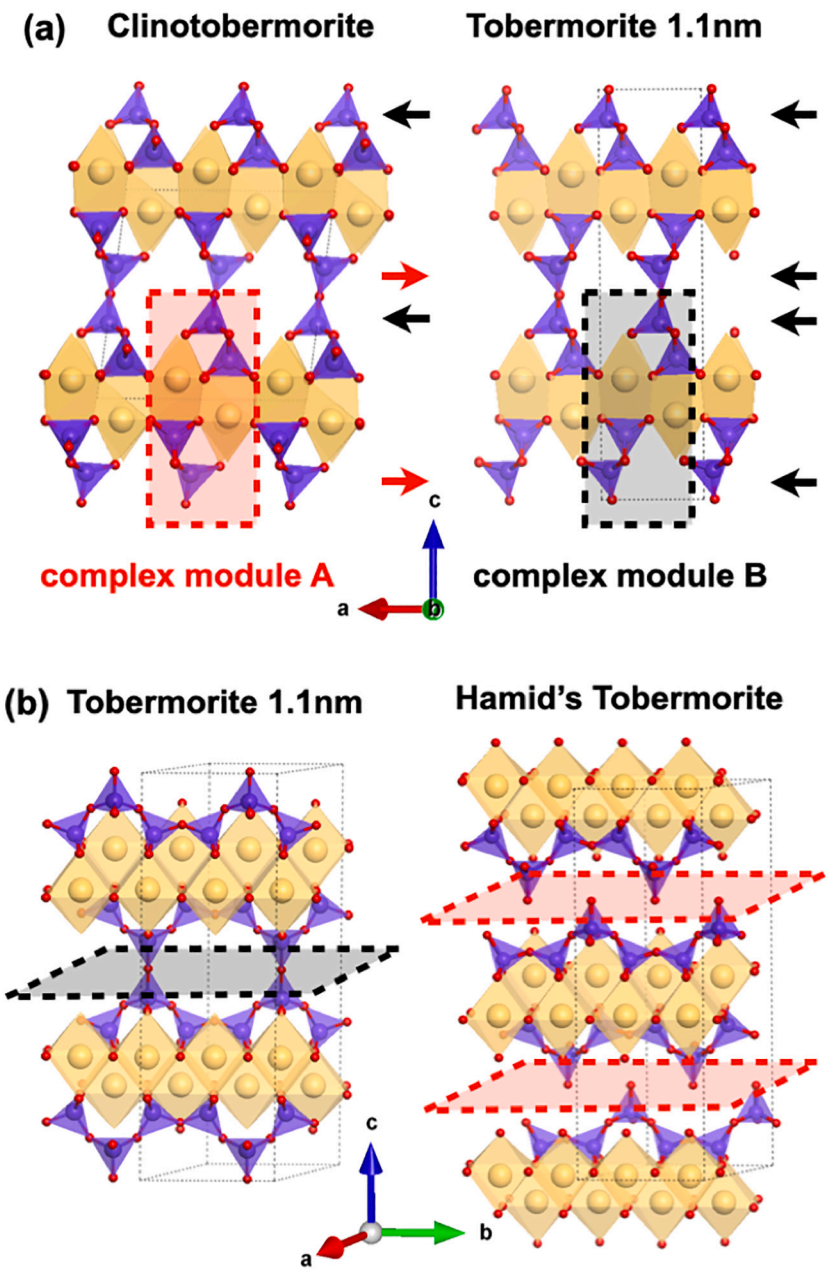

Fig. 2. (a) Crystalline structure of the clinotobermorite and tobermorite. The arrows indicate the orientation of the bridging silicate tetrahedral. (b) Tobermorite 1.1 nm and Hamid's tobermorite. The interlayer spaces are shown to guide the eye to the differences between both structures. The colour code is the same as in Fig. 1.

In the 1990s, a general model was proposed by Richardson and Groves [52–54] based on the stoichiometry of tobermorite, jennite, and portlandite. This model pictures the C-S-H gel as finite silicate chains following the $3n - 1$, joined to calcium hydroxide layers, to form structures that locally can resemble tobermorite, jennite, or portlandite. The C-S-H gel could be then a mixture of tobermorite-like regions and jennite-like or portlandite regions. They also introduced a variable protonation of the silicate chains and considered the presence of a variable amount of calcium and hydroxyl groups in the interlayer space to compensate for the charge imbalance [52]. The formulation of the C-S-H proposed in this model includes possible substitutions or incorporations of guest ions [54,55]. They wrote a general stoichiometric formula by considering the different structural units of their model:

$$\left[Ca_{2n}H_w\left(Si_{1-a}R_a\right)_{3n-1}O_{9n-2}\right]I^{c+}_{\frac{q}{c}(3n-1)}(OH)_{w+n(y-2)}Ca_{\frac{my}{2}}\cdot mH_2O \quad (1)$$

where the number of silanol groups is given by w and the degree of protonation is defined as w/n. The term in braces corresponds to the calcium and silicate layers, while the other terms are extra ions and water. R is referred to trivalent ions, such as aluminum, that substitute bridging silicon ions, I represent the monovalent or divalent cations that ensure the electroneutrality after aliovalent substitutions and c is the formal charge of these cations. This formula is extremely flexible and can virtually fit with any possible set of defects that the atomic structure of a C-S-H model based on tobermorite could have. Taylor in [17] recognized that the model of Richardson and Groves was more general than his own attempts, yet he described it as "a constitutional rather than a structural model; that is, it deals with the nature and relative proportions of the ions present but not in any detail with how these are arranged". Nevertheless, in a series of following works Richardson focused on the discussion of structural aspects of the C-S-H (and C-A-S-H) atomic structures within the original model stoichiometry for a wide range of samples and conditions [20,53,56–59].

Many other models and refinements have been proposed after the one of Richardson and Groves. Most of them fit within the general formulation by Richardson and Groves and describe particular structures, or structural motifs, that match with experimental observations. For instance, Cong, Kirkpatrick, and coworkers [13,41,60] proposed a C-S-H model based on defective tobermorite-like structure, suggesting that jennite-like features are not present or are negligible at best. Their model was therefore limited to Ca/Si ratios below 1.5. The model proposed by Nonat et al. [61,62] was also based only on tobermorite, but unlike Cong and Kirkpatrick's model, it covers a wider range of Ca/Si ratios. It stresses that the C-S-H structure at high Ca/Si ratios can be achieved in tobermorite by introducing interlaminar calcium hydroxide and that the C-S-H may not be as disordered as previously suggested. He also classified the C-S-H in three differentiated products that form at well defined Ca/Si ratios: α-C-S-H (0.66 V Ca/Si < 1), β-C-S-H (1 < Ca/Si < 1.5) and γ-C-S-H (1.5 < Ca/Si < 2). More recently, Gartner and Maruyama [63] used a structural model similar to the previous ones, but emphasizing the importance of the interlaminar calcium ion and its solvation shell on the formation and shrinkage of the C-S-H gel. Chen et al. and Kulik [64,65] used solubility and thermodynamic data to suggest specific compositions and structures for different Ca/Si ranges, yet compatible with the general Richardson-Groves stoichiometry.

Despite the general agreement in the community with Taylor's model and Richardson's stoichiometric formulation, alternatives have been also suggested. Grutzeck proposed in 1999 a sorosilicate C-S-H model, with an initial cuspidine-like structure that may evolve to *dreierketten* chains by diffusion-controlled phase change [66,67]. Very recently, some authors have proposed independently a model in which tobermorite-like layers and portlandite mono- or bi-layers coexist [19,34]. In their studies, they calculated the pair distribution function from high-energy X-ray experiments, Grangeon et al. for C-S-H samples with Ca/Si ratio below 1.5 [34] and Cuesta et al. for samples from alite hydration [19]. Both found that, in order to match the experimental pair distribution function, they should add the signal of portlandite layers to that of clinotobermorite. Grangeon et al. specified that the coexistence must be considered for Ca/Si ratios >1.23, and both monolayers and bilayers of portlandite seem to be present. [34]. Cuesta et al. that the portlandite monolayer should be stretched for a perfect match of the PDF. This new evidences would imply a reconsideration of the accepted tobermorite-like model, bringing back the possibility of a mixed tobermorite/portlandite C-S-H. It must be kept in mind that Richardson's stoichiometric formulation still describes the tobermorite/portlandite structures. Overall, it is clear that the atomic structure of the C-S-H is still far from being settled unequivocally.

4. Computational models of C-S-H gel

This section summarizes the main achievements and milestones in the development of C-S-H gel atomistic structural models. The complexity of the problem lies in the non-crystalline atomic structure. For crystalline materials, the atomic positions can be unequivocally determined using X-ray diffraction experiments. Even if crystals often include point defects like vacancies or substitutions and line defects like dislocations, the ideal atomic structure is available as starting point [68]. That is not the case for C-S-H, and the definition of the initial structure is a problem itself. We divided the models into “early” and “current” models. The former do not reproduce some of the C-S-H more important characteristics of the gel-like, yet they can be used as idealized versions or model systems for specific purposes. The latter are more complex models that include most of the C-S-H structural information.

4.1. Early C-S-H computational models

In 1996, Faucon et al. [69,70] carried out the first study of the C-S-H structure employing molecular dynamics. Their work aimed to evaluate the breaking mechanisms of the C-S-H chains and identify the sources of its structural instability. For that purpose, they built two systems based on the structure of tobermorite 1.1 nm proposed by Hamid [30] that differed in the Ca/Si ratios: 0.66 and 0.83. The Ca/Si ratio of 0.83 was achieved by the substitution of two protons of the tobermorite 1.1 nm structure by a Ca ion. At Ca/Si = 0.66, no break in the silicate chains was observed when the model was relaxed at 800 K. In contrast, the substitution of $2H^+$ by Ca^{2+} to reach a Ca/Si ratio of 0.83 resulted in a partial rupture of the silicate chains due to the formation of Si-O-Ca bonds. In this work, Faucon and coworkers also analyzed the stability of Al substitution in pairing and bridging sites, which is treated in Section 5.1.

A few years later, in 2002, Kalinichev and Kirkpatrick [71] employed molecular dynamics to study the adsorption mechanisms of chloride anions at the surface of different minerals. In particular, they used tobermorite 0.9 nm as a model for C-S-H gel. They used the ClayFF force field [72] to describe the metal-oxygen interactions, which enables the mobility and flexibility of hydroxyl groups from the surface. They found very low chloride sorption capacity in tobermorite 0.9 nm and the authors suggested that the chloride sorption capacity for C-S-H should be even lower, since the simulated tobermorite model contained a full set of Si-OH surface sites, while those sites are mainly deprotonated at higher Ca/Si ratios and pH. The extra negative charge due to this deprotonation should provoke high repulsion of chloride anions. Later on, these authors employed the same approach to study in detail the structure, dynamics, and energetics of water confined in C-S-H [73]. Again, the structure of non-modified tobermorite 0.9 nm was employed as a model for C-S-H, and different pore sizes were considered, constituting the first molecular dynamics models to study C-S-H pores. The molecular dynamics simulations showed high structuring of water molecules and the development of a hydrogen bond network between the water molecules and the surface. The authors suggested that the degree of depolymerization of the silicate chains and the deprotonation of pairing Si-OH in C-S-H might cause distortions on the water structure and lead to lower diffusion coefficients regarding tobermorite due to hydrogen bonding with surface dangling atoms.

In 2004, Gmira et al. [74] employed empirical potentials and *ab initio* methods to investigate the nature of the interatomic forces as well as the elasticity in the structures of tobermorite 1.1 nm defined by Hamid [30] and Merlino [27]. Changing the basal distance for a fixed interlayer water and Ca content they identified three energy minima between 1.0 and 1.4 nm and showed that the cohesion in C-S-H is essentially due to the electrostatic forces and the iono-covalent forces caused by the Ca ions and water in the interlayer.

The first attempt to build a computational C-S-H model by cutting the silicate chains of tobermorite 1.4 nm and jennite minerals was done in 2007 by Manzano et al. [75,76]. This C-S-H model consisted of a mixture of dimers, pentamers, and octamers obtained by omitting bridging tetrahedra in the infinite silicate chains of tobermorite 1.4 nm and jennite minerals. The charge defects introduced in the crystalline structure of those minerals were compensated by introducing protons in the terminal oxygen atoms of the finite silicate chains, while the water and Ca contents remained unchanged. The obtained models are defective crystals rather than disordered C-S-H, as periodicity was kept in the unit cell, yet the authors showed that they were reasonable approaches to study the dependence of the elastic properties of C-S-H gel with respect to its composition and silicate chain length. The results showed that the mechanical properties increase as the chain length grows due to the higher stability of longer silicate chains. The elastic properties of the proposed C-S-H models were considerably lower than for the perfect crystals of tobermorite 1.4 nm and jennite, and in good agreement with the experimental nanoindentation measurements once nanoporosity was taken into account by poromechanical models.

Also in 2007, Dolado et al. [77] published a radically different approach to model C-S-H. Instead of using tobermorite as a C-S-H model, they performed molecular dynamics study to simulate the polymerization of silicic acids in a Ca-rich environment. They employed the Litton

and Garofalini potential for amorphous glasses [78] at very high temperatures (>1500*K*). They observed that the polymerization was faster at lower Ca/Si ratios and that the appearance of three-dimensional structures, like branched silicate and rings, decreases as the Ca/Si ratio increases. Thus, the presence of Ca ions not only slows down the polymerization of the silicate chains, but also enforces the formation of linear structures. Likewise, they measured the silicate chain lengths, finding that the higher the Ca/Si ratio, the shorter the silicate chains. However, the resulting structure must be considered a calcium silicate glass rather than C-S-H, as they did not observe any local order or formation of calcium silicate layers.

4.2. Current C-S-H computational models

Hitherto, most C-S-H models were essentially crystalline tobermorite or slightly modified variants. They were a reasonable first approach, but some of their basic features were not compatible with the characteristics of real C-S-H. For instance, the density and Ca/Si ratio are considerably higher in C-S-H ($\rho_m = 2.6$ g·cm^{-3} and Ca/Si = 1.7 [14]) than in tobermorite ($\rho_m = 2.23$ g·cm^{-3} and Ca/Si = 0.83 [79]) and jennite ($\rho_m = 2.32$ g·cm^{-3} and Ca/Si = 1.5 [80]) minerals. For that reason, in 2009, Pellenq et al. [81] employed a new approach to develop the first disordered C-S-H model. They took the unit cell of dry tobermorite 1.1 nm as a starting point to build a disordered C-S-H by introducing several modifications.

- In the first step, all water molecules were deleted and the specified Ca/Si ratio, 1.7, was achieved by shortening the silicate chains by removing neutral SiO_2 groups in order to obtain a defective C-S-H structure matching the experimental Q^0, Q^1, and Q^2 distribution given by experimental NMR analysis [60,82].
- Ca was introduced to compensate for the charge imbalance provoked by the SiO_2 deletion.
- Then, the structure was relaxed, obtaining a distorted layered structure.
- To reintroduce water, Grand Canonical Monte Carlo (GCMC) simulation was performed, coupling the C-S-H structure to an external water reservoir at the chemical potential of liquid water at 300 K. Water entered into the original interlaminar space, but also in new spaces created by the omission of silicate groups, reaching a density of 2.56 g·cm^{-3}, close to the experimental one (2.6 g·cm^{-3}) obtained by small-angle neutron scattering (SANS) measurements [14].
- Finally, the structure of the system was further relaxed under constant pressure and temperature, which caused an expansion of the interlaminar space and the density was reduced up to a final value of 2.45 g·cm^{-3}.

The chemical composition of the final structure was $(CaO)_{1.65}(SiO_2)(H_2O)_{1.75}$, very close to the experimental average composition [14] $(CaO)_{1.7}(SiO_2)(H_2O)_{1.8}$. It is remarkable that the final structure had a similar amount of water to tobermorite 1.4 nm, but in this model, water is packed randomly in the interlayer space due to the presence of defects in the silicate chains, which reduces the basal distance. The model was validated by comparison of structural and physical properties with experimental measurements obtained by X-ray absorption fine structure (EXAFS) [83], X-ray diffraction (XRD) [84], and infrared spectroscopy (IR) [13]. It must be noticed that the experimental EXAFS and XRD C-S-H samples have lower Ca/Si ratios than the model (1.4 and 1.1, respectively), and the comparisons serve to prove only qualitatively the disordered nature of the C-S-H model. Furthermore, this model was used to calculate mechanical properties, such as mechanical stiffness, strength, and hydrolytic shear response, obtaining results in good agreement with the experimental nanoindentation values [85,86]. The results given by this model suggested that the C-S-H have both glass-like short-range order and crystalline features from tobermorite [81].

This model was a great step forward in the modeling of C-S-H gel, although it was never bereft of controversy due to its inconsistencies. Indeed, some authors criticized the C-S-H model proposed by Pellenq. Thomas et al. [88] highlighted that the model density was in better agreement with experiments than crystalline tobermorite, but still quite far from real C-S-H gel. Richardson [89] also criticized it because the Ca—O distances were either shorter or longer than the measured Ca—O distances in calcium silicate hydrates and related phases by X-ray diffraction (XRD). Moreover, he also pointed out that more than half of the Ca atoms were undercoordinated, bonded to less than six oxygen atoms. The main point of disagreement was the structure of the silicate chains. The model has a Q^n distribution ($Q^0 = 13\%$, $Q^1 = 67\%$ and $Q^2 = 20\%$), similar to that of experimental samples (Q^0 ~10%, Q^1 ~67% and Q^2 ~23%). However, the experiments included the Q^0 sites due to the contribution of unhydrated C_3S, and not present in C-S-H [62,90].

Despite the criticism and inconsistencies of the C-S-H model developed by Pellenq and coworkers [81], it is possibly the biggest milestone for the description of the C-S-H using molecular scale modeling. It showed that it was possible to build more realistic models than tobermorite and lead to an increasing number of studies and model improvements. For instance, in 2012, Manzano et al. [91] refined the model enabling the dissociation of water molecules confined in C-S-H micropores. For that purpose, they used a reactive force field, ReaxFF [92,93]. They did not observe water dissociation during the energy minimization at 0 K, but as soon as the system was transferred to the canonical ensemble at 300 K, the dissociation occurs, producing the ionic pair OH^--H^+. The process of dissociation is very fast, taking place within the first 0.2 ns of MD simulation. The protons react only with nonbridging oxygen atoms of the silicate chains, while the hydroxyl groups coordinate to interlaminar Ca ions, forming Si-OH and Ca-OH groups. Almost half of the original water content was dissociated, becoming a constitutive part of the C-S-H gel. It should be pointed out that no other reactions took place besides the dissociation of water molecules, so the silicate monomers did not react to form longer chains. For that reason, the authors concluded that the monomers trapped during the nucleation process may remain stable. After the water dissociation, the overall density of the system increases. The authors, based on the analysis of the arrangement structure, attributed this growth to the formation of hydroxyl groups, which induces a decrease of the long-range order, leading to a configuration more disordered and favorable energetically.

In 2014, Abdolhosseini Qomi et al. [87] introduced a second improvement to the C-S-H model of Pellenq et al. (see Fig. 3), which solved some inaccuracies criticized by other authors. The building scheme is similar to the original one from Pellenq's model [81], yet the amount of Q_0 sites is zero for low Ca/Si ratios, and kept close to zero for high Ca/Si ratios. They also included a molecular dynamics step with the reactive force field ReaxFF [92,93] at 500 K, allowing the dissociation of water molecules. Then, the systems are transferred to a non-reactive environment using the CSH-FF force field [94] due to the high computational cost of ReaxFF. Using this non-reactive force field, the annealing of the sample is simulated reducing the temperature from 500 to 300 K along 3 ns at ambient pressure. In this way Abdolhosseini Qomi et al. [87] built about 1500 C-S-H gel configurations with a broad range of compositions, spanning Ca/Si ratios between 1.1 and 2.1. It should be noted that for Ca/Si ratios higher than 1.5, pairing silicates are removed and some monomers are created in the C-S-H structure, although some of them condensated during the MD simulation with ReaxFF. The aim of the authors was to build a database of atomic configurations of C-S-H validated with structural and mechanical data and classify them according to three defect attributes: Ca/Si ratios and correlation distances for medium-range Si—O and Ca—O environments [87]. In this way, it is possible to establish a structure-property correlation, enabling the screening of the database for the desired properties against the defect attribute.

In 2015, Kovačević et al. [95] proposed three models for the structure of C-S-H gel based on tobermorite 1.1 nm. They developed a large

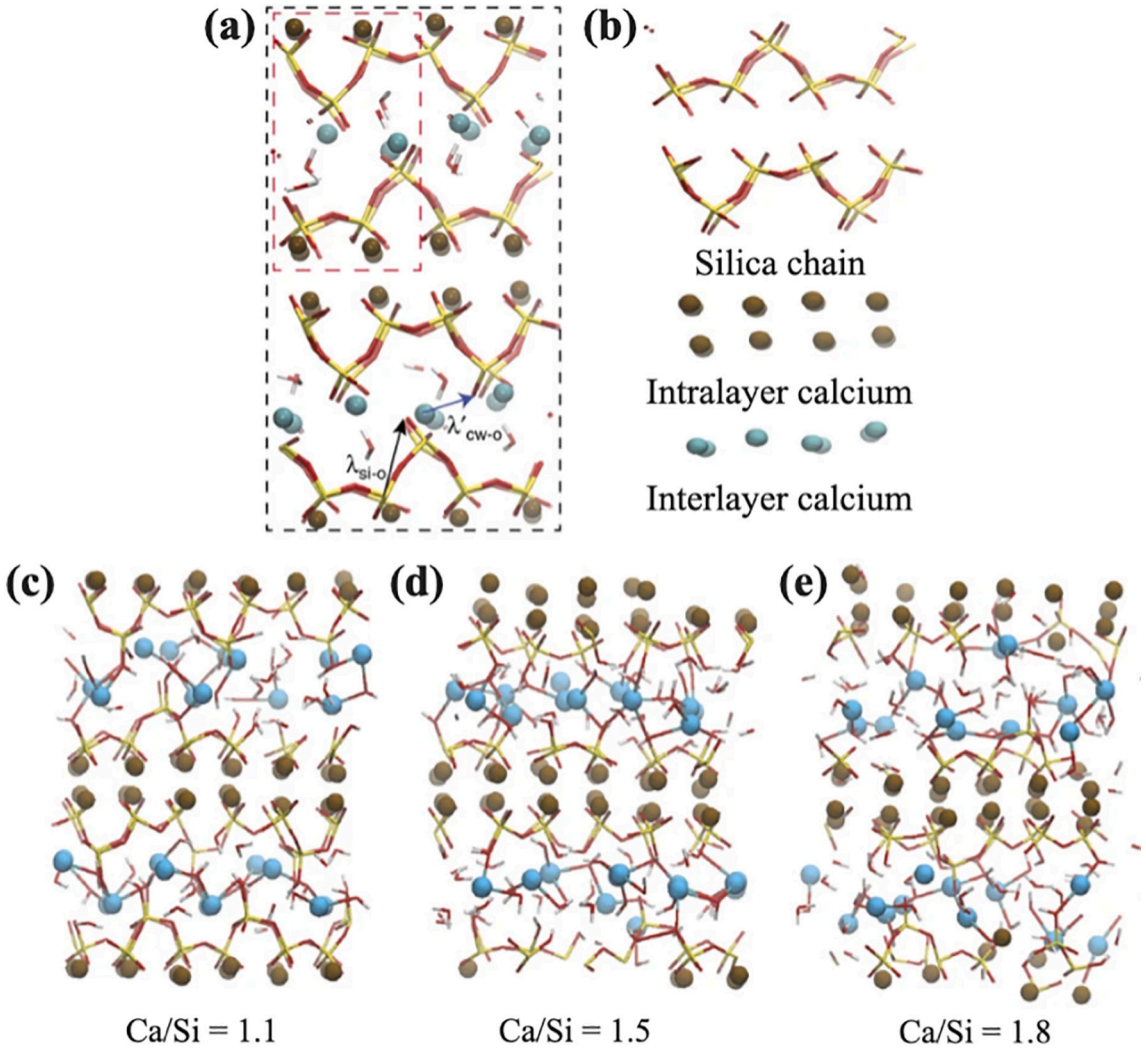

Fig. 3. The refinement of Pellenq's defective tobermorite models by Qomi et al. (a) Structure of tobermorite 1.1 nm was used as a baseline to build the C-S-H models. (b) Components of tobermorite: silicate chains (above), intralayer calcium (medium), and interlayer calcium (below). Atomic structure of C-S-H models with Ca/Si ratios of (c) 1.1, (d) 1.5, and (e) 1.8. Adapted by permission from SpringerNature, [87], Copyright 2014.

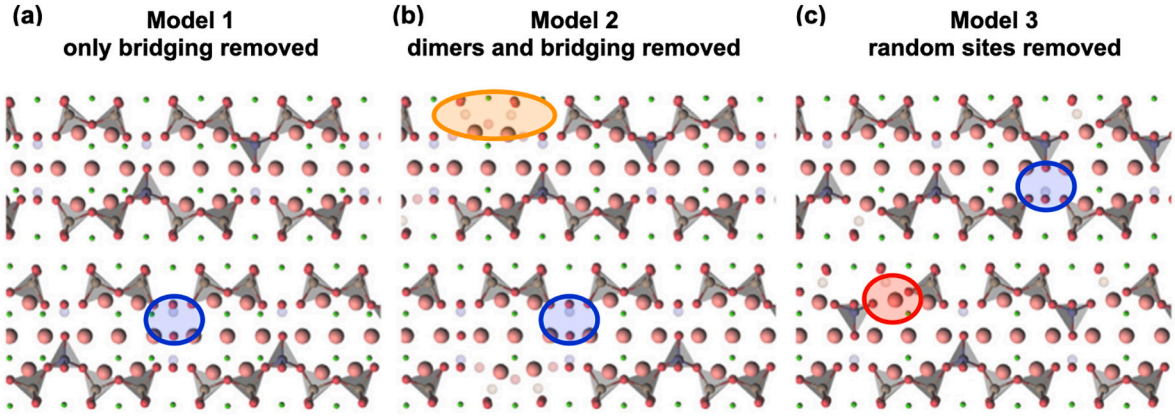

Fig. 4. Proposed models by Kovačević and coworkers for the structure of C-S-H gel with Ca/Si ratio 1.68, corresponding to (a) model 1, (b) model 2, and (c) model 3 (see text). The colored regions show examples of which type of site was removed in each model: blue for bridging sites, orange for dimers, and red for pairing sites. Adapted from [95], Copyright 2021, with permission from Elsevier. (For interpretation of the references to colour in this figure legend, the reader is referred to the web version of this article.)

number of configurations with a random distribution of variable-size silica oligomers for each model. As a starting point, they employed the structure of tobermorite 1.1 nm described by Merlino et al. [27], while Pellenq-type models [81,87] employed Hamid's tobermorite 1.1 nm [30]. The three different models arise from the strategy followed to increase the Ca/Si ratio up to 1.68. This can be achieved by the addition of Ca ions and/or the removal of SiO_2 groups. In short, the three models were done by:

- Model 1: Removal of bridging SiO_2 sites, controlling the length of the silicate chains to follow the 3n-1 rule and adding Ca in the interlayer space. In this way, the C-S-H model is composed of dimers and pentamers, without the presence of monomers (Fig. 4a).
- Model 2: Removal of bridging SiO_2 sites + SiO_2 dimers and adding Ca in the interlayer space. This combination obeys the 3n-1 rule, yet leads to areas of the calcium oxide layer exposed to the interlaminar space (Fig. 4b).
- Model 3: Random deletion of bridging and pairing silicate tetrahedrons (Fig. 4c). Therefore, there are monomeric silicates in the structure of C-S-H, and the 3n-1 rule is not fulfilled.

Following this procedure, they generated a great number of C-S-H structures, more than a thousand structures in total, at the same Ca/Si ratio (1.68) and for H/Si ratios from 1.3 to 2.3. All those configurations were relaxed and then, molecular dynamics simulations were performed using the ReaxFF force field in order to estimate their bulk densities and total energies. The models and their configurations do not have the same stoichiometry and they also contain different amounts of water, inserted by Grand Canonical Monte Carlo, which complicates the interpretation of the results. The calculated total energies are rescaled to make them comparable, resulting in significant energy differences between the three models. The first model exhibits the lowest energy, suggesting that it is the most probable one. Furthermore, the analysis of the bulk density of the samples shows that the first model has the highest corrected density (2.76 $g{\cdot}cm^{-3}$ for H/Si ratio of 1.8), very close to the experimental value (2.6 $g{\cdot}cm^{-3}$). In this way, the first model, based on the combination of the incorporation of Ca ions and random deletion of bridging silicates that forms dimers and pentamers, results in the most stable model and with a density value that matches the experimental one. The building strategy and resulting structure could be considered as the same one achieved by Pellenq-type models [81,87], correcting the presence of silicate monomers, whose presence is not supported by experimental studies [62,90]. Despite the clear conclusions of this work, other researchers have continued using models with missing pairing sites to explore the effect of the silicate chain structure on the C-S-H properties [96].

The C-S-H computational model proposed by Mohamed et al. in 2018 [97] is a radically different approach to C-S-H construction. It is based on the experimental synthesis and characterization of C-S-H samples at a wide range of Ca/Si ratios reported in [8]. From the point of view of the C-S-H atomic structure and stoichiometry, the model is not that different from the previous ones. Its main characteristic is that Ca ions are incorporated in well defined positions as bridges of terminal silicates Q^1 of the chains, rather than randomly in the interlayer space. The authors claimed that the presence of those bridging Ca, together with the hydrogen bond network, contributes to the stabilization of the C-S-H structure, which is particularly important at high Ca/Si ratios. The process to evolve from tobermorite to a more realistic structure of C-S-H starts with the deprotonation of the silanol groups of the bridging silicates, which is compensated by the incorporation of $Ca(OH)^+$ ions. Then, the bridging silicate tetrahedrons are deleted and the

(a)

Code	Unit	Stoichiometry	Charge	Code	Unit	Stoichiometry	Charge
Ca-Si sheet above interlayer				Ca-Si sheet below interlayer			
<		$CaSiO_{3.5}$	-1	>		$CaSiO_{3.5}$	-1
S		SiO_2	0	S		SiO_2	0
[S]'		[SiO]H	+1	[S]'		[SiO]H	+1
/		$Ca(OH)_2$	0	\		$Ca(OH)_2$	0
(		$CaSiO_4$	-2	)		$CaSiO_4$	-2
S|		$SiO_{1.5}$	+1	|S		$SiO_{1.5}$	+1
[		$Ca(OH)_{1.5}$	+0.5	]		$Ca(OH)_{1.5}$	+0.5
interlayer							
C		Ca	+2	°	°	OH	-1
1		H_2O	0				

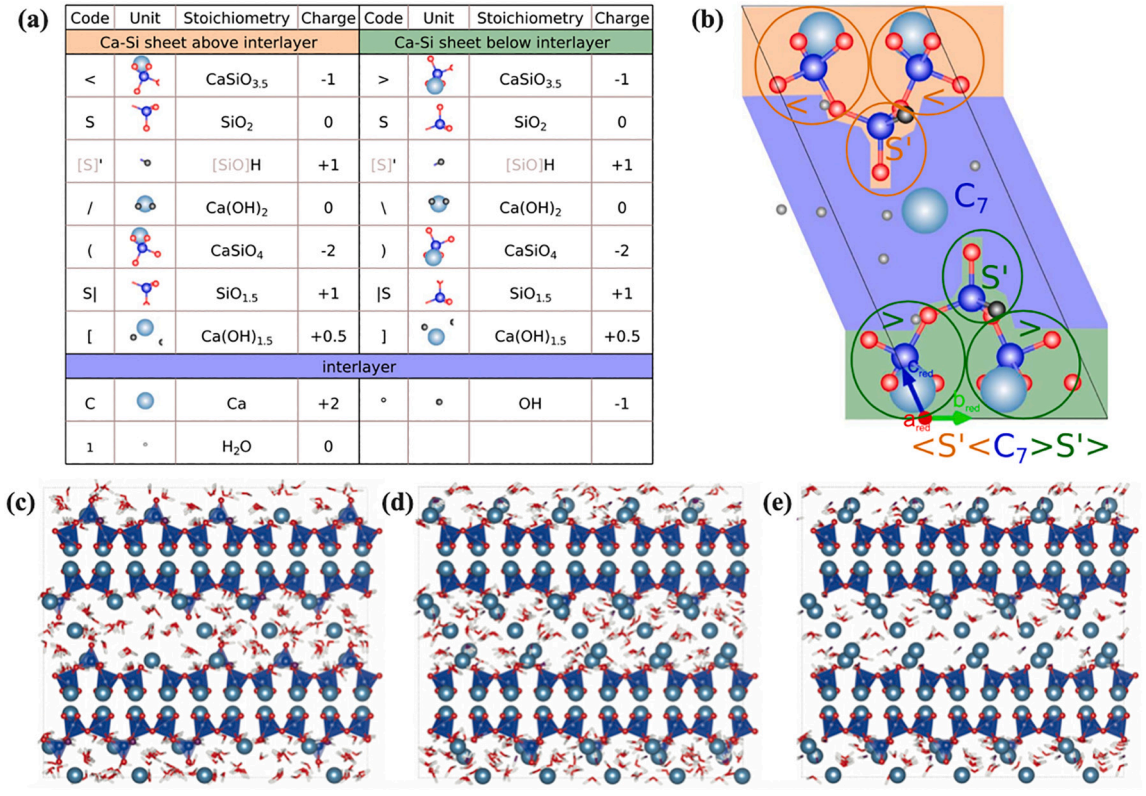

Fig. 5. (a) Definition and notation of motifs employed in the brick C-S-H model. (b) Example of a brick built from the motifs in (a). In this case, the brick represents the primitive unit cell of 1.4 nm tobermorite, using the motifs corresponding to the code <S′<C7 > S′>. Adapted from [97], Copyright (2018), with permission from Elsevier. C-S-H structures proposed by Kumar et al. for the C-S-H structure with Ca/Si ratios of (c) 1.25, (d) 1.75, and (e) 2.0 viewed along the [100] direction. Adapted from [8] Copyright (2018) with permission from American Chemical Society.

electroneutrality is maintained by adding two protons, one proton and one $Ca(OH)^{+}$, or one Ca^{+2} ion, coordinated to the bridging sites. Extra $Ca(OH)_2$ groups can be added to increase the Ca/Si ratio if necessary.

From a computational point of view, the construction method is completely different from the previous works. Starting from tobermorite, Mohamed et al. defined a collection of basic building blocks covering a range of possible irreducible motifs within the C-S-H (Fig. 5 a). Those building blocks are then combined to form different unit cells or "bricks" (Fig. 5 b), which are checked after a DFT energy minimization, evaluating the Ca—O distances, the coordination number of Ca ions, and local charge neutrality after relaxation. The bricks that satisfy the structural checking are then combined to form a variety of C-S-H structures with different structures and/or compositions (Fig. 5 c). A variable amount of interlayer $Ca(OH)_2$ and water molecules can also be specified as additional bricks, but it is not very clear how these motifs are placed. The authors show how the brick-by-brick building scheme can reproduce tobermorite and jennite crystals, as well as and previous C-S-H models. It is flexible enough to create multiple structures with Ca/Si ratios from 1.0 to 2.0, with point defects, stacking faults, different protonation degrees of the silicate chains, etc. They also propose specific blocks to reproduce C-S-H surfaces, an innovative approach to study systematically C-S-H interfacial properties. In a recent paper [98] the authors extended further the collection of building blocks adding Al, expanding the available chemical space to include C-A-S-H.

Since the development of the previous models, most works have focused on their application to compute nanoscale properties, yet recent studies related to structural refinements have also been done. For instance, comparing DFT simulated and experimental XRD patterns of synthetic C-S-H with a Ca/Si = 1, Basquiroto de Souza et al. suggested that the C-S-H structure is less disordered than the proposed by other models, and that the stacking disorder is a key factor to take into account [99]. Although the basic pillars of the C-S-H models are well established, there is still room for improvement and refinement.

4.3. C-S-H surfaces and pore models

In Section 5, we will see that a large part of the applications of atomistic C-S-H models is related to interfacial properties and nanopores. Therefore, it is relevant to review how C-S-H surface models are built.

The C-S-H surface and pore models are built following the standard practices in atomistic simulations: a two dimensional slab is created by "splitting" a bulk system through a given crystallographic plane, introducing a "vacuum layer". The plane must be chosen carefully to avoid, when possible, breaking covalent bonds, maintaining the highest possible coordination numbers, and avoiding charged slabs (see the Tasker surface classification for more details [100]). In the case of the C-S-H gel, given the tobermorite-like layered structure, the researchers have adopted the practices from the clay community, introduced mainly by Kalinichev et al. [71]. Clay particles are formed by the stacking of independent layers, with variable water content and ionic composition in the interlayer space. The direction perpendicular to the layers is therefore the most obvious choice to create the surface: it is the main surface in terms of exposed area, and chemically stable due to the lack of dangling bonds. The "vacuum layer" can then be saturated with water, organic molecules, ionic solutions, etc. [101–106].

Nevertheless, there are important differences between clays and the C-S-H, due to the non-crystalline nature of the latter. In clays, the surfaces are unequivocally determined by the crystallographic structure, with no dangling bonds. In the case of the C-S-H gel, surfaces will have a random composition and structure, and will have dangling bonds from the finite silicate chains, just like the bulk. The surface (or interfacial) structure will vary depending on the pore solution chemistry and especially with the pH. However, the vast majority of reported works do not take into account this point, and the surfaces have the same structure as the bulk layers. The impact of such an approximation is difficult to evaluate, and considerably more work will be necessary. Among the few attempts done so far, Jamil et al. computed using MD simulations the surface and solid-water interfacial energies of different tobermorite planes. In agreement with the previous discussion, the (001) direction with the surface coinciding with the tobermorite layers is the most favorable one, with negligible interfacial energy [107]. However, other surfaces also present very low surface energy, especially the (100), making them relevant. In addition, the authors explore the hydroxyl group density on the surfaces and the associated approximate pH. Yet the system is tobermorite and not a C-S-H model, the concepts introduced to show that other surfaces than the (001) cannot be discarded and that the surface chemistry should be taken into account. Another interesting approach has been proposed, although not explored in detail, in the framework of the brick model [97]. The authors suggested that specific bricks could be constructed to reproduce surface states. That opens the possibility of creating surface compositions and hydroxylation states independent of the bulk composition.

5. Applications of the C-S-H computational models

In this section, we review some of the most prominent applications of the C-S-H computational models. In many cases, we include paper "early models" to show the evolution of the field, even though they cannot be strictly considered C-S-H models, as we will discuss later.

5.1. Al-incorporation into the C-S-H gel

The determination of aluminum preferential incorporation sites into the C-S-H gel has been probably the most successful application of atomistic simulations in cement research, as atomistic simulation has reproduced the experimental observations in most cases. It is also an interesting example of how the atomistic models have evolved from very simple cluster models to the current complex models. Briefly, experimental studies using Si-NMR and Al-NMR proved that tetra-coordinated aluminum, Al(IV), is incorporated into the C-S-H gel silicate chains in the bridging site [108–113]. As a consequence, dimers merge into pentamers and longer aluminosilicate mean chain lengths (MCL) are observed. For low Ca/(Si + Al) ratios, Al(IV) enhances interlaminar chain cross-links via condensation of bridging sites, forming zeolite-like cavities as in tobermorite 1.1 nm and clinotobermorite.

The first attempt to investigate the aluminum incorporation into tobermorite was done in 1994 by Kashihara et al. [114]. They aimed to study the tobermorite 1.1 nm case using a cluster model and ab initio simulations. Likely, some methodological flaws (like charge imbalance due to the substitution) and computational power limitations did not allow a proper energy minimization, and their simulations predict the lowest substitution energy for pairing sites.

Manzano et al. used an even simpler model, testing with Density Functional Theory (DFT) the Si for Al substitution energy in a 5-membered silicate chain isolated from tobermorite 1.4 nm [115]. The heavy atoms (Si and Al) were frozen to maintain a *dreierketten* arrangement, while O and H were relaxed. The calculated aluminosilicate condensation energies, Al for Si substitution energies, and cluster stability index indicated that the bridging site is preferred over pairing and ending sites. The suggested reason was a better stabilization of the electronic structure and charge localization when Al was located in the bridging site. The pairing site and ending sites were energetically less favorable than the bridging by 4 and 21 $kcal \cdot mol^{-1}$ respectively.

Pegado et al. also computed the substitution energies with DFT methodology, yet in a more complex model consisting of a single tobermorite layer isolated from the crystal 116. Some bridging sites from the silicate chains were removed, creating finite chains, and multiple possible Al for Si substitutions were analyzed for good statistical analysis. Essentially, they reach the same conclusion as [115], with the bridging site as the most favorable from a thermodynamic point of view, followed by the pairing and the ending sites. However, the energy

penalty for the pairing site was close to that of the ending site. The values with respect to the most favorable conformation were 20 and 25 kcal·mol^{-1} for pairing and ending sites respectively. The result suggests that the presence of the calcium oxide layer has an important role in the instability of Al incorporation into the silicate chains that the cluster model could not reproduce.

For more complex models ab initio simulations are computationally too expensive, and molecular dynamics (MD) with empirical force fields are used (see Fig. 7). The first MD work, done in 1997 by Faucon et al. [70], aimed to evaluate the stability of Al substitution in bridging and pairing sites using two models based on the structure of Hamid's tobermorite [30], in which Si is partially substituted by Al. These models had a Ca/(Si + Al) ratio of 0.83 and Al/Si ratio of 0.3 and they differed in the position of the aluminum substitution: only in the bridging positions, or half in the bridging sites and the other half in non-bridging sites. The charge imbalance caused by these substitutions was compensated by the protonation of non-bridging oxygen atoms of the silicate chains. The relaxation of the model with aluminum only at bridging sites was stable, while there were occasional ruptures of the aluminosilicate chains in the mixed substitution model. The study suggested that these ruptures were caused by the poor charge compensation in the chains since the charge of aluminum in pair sites could not be locally balanced by protons.

Manzano et al. [118] investigated the polymerization process following the same approach as [77], but in presence of aluminum. They considered systems at different Al/Si ratios, up to 0.33, and Ca/Si ratios from 0.95 to 2.0. They found that both the amount of Q^3 and Q^4 species and the MCL increase as the Al/ content increases. The analysis of the occupancy of the Al atoms within the C-S-H structure shows a negligible amount of Al in Q^1 sites, especially at low Al/Si ratios for any Ca/Si ratios. The incorporation of Al to the polymerization favored the formation of three-dimensional structures and longer chains. However, for high Al/Si ratios and high Ca/Si ratios, the fraction of Al in paired and ending sites increased. As mentioned before, it must be noted that the type of structures formed in these simulations are more similar to glasses than to the C-S-H, as the layered structure is not developed [77].

Regarding more realistic C-S-H models, Abdolhosseini Qomi et al. used also the core-shell force field to study the Al substitution into the C-S-H model developed by Pellenq and coworkers [117]. The results followed the same trend as in ab initio simulations, with the bridging site as the most stable one, followed by the pairing (+300 kcal·mol^{-1}), and being the ending position the less stable (+430 kcal·mol^{-1}). The energy differences must be seen as qualitative since the core-shell potential overestimates the energy difference between configurations [119]. Abdolhosseini Qomi et al. also predicted a small expansion of the interlayer space, less than 3%, due to the incorporation of counter-balancing ions. They also suggested the possible existence of Al(V) and Al(VI) in a position that could be interpreted as a bridging site between chains by overcoordination of Al(IV) by OH groups and water.

Recently, Kuhni Mohamed et al. deepen into the presence of Al(IV) of bridging sites [98]. They incorporated Al into their brick model and performed DFT simulations to analyze the coordination and stability of Al as a function of the Ca/Si ratio. They also computed the NMR chemical shifts and compare them with experiments. They concluded that the Al(IV) is the most stable form at low Ca/Si ratios, but upon increasing the Ca concentration, and consequently, the number of hydroxyl groups, Al evolves to a six-fold coordinated $[AlO_2(OH)_4]^{5-}$ specie, while maintaining its position at the bridging sites. Their computational results, together with dynamic nuclear polarization (DNP) NMR experiments, made them conclude that the TAH phase (third aluminate hydrate) does not exist. TAH was proposed to be a disordered aluminum hydroxide or calcium aluminate hydrate originating the Al(VI) NMR signal [108,109].

5.2. Elasticity and mechanical properties

The calculation of elastic and mechanical properties of the C-S-H has probably been the more explored topic by atomistic simulations. Once an appropriate C-S-H model was developed, it has been relatively easy to investigate its mechanical performance under tensile or shear deformations, investigate the effect of temperature, water content, chemical substitutions, etc. Below we review some of the main advances, yet many more papers are been published on this topic in recent years [120–126].

In 2009, Manzano et al. [76] were among the first to study elastic properties of main phases in Portland cement pastes by modeling them with a classical force field in the core-shell approach. They derived bulk (K) and shear (G) moduli in the averaged Hill approach from computed elastic constants and used them to access the average Young's modulus (E=$9G/(3 + G/K)$) and Poisson's ratio (ν=$(3 - 2G/K)/(6 + 2G/K)$) assuming isotropic media. Values are reported in Table 1 as Ref. 76. They used an "early model" for the C-S-H, with crystalline tobermorite and jennite crystal having either dimeric, pentameric, or octameric silica chains. Their results highlighted the fundamental role silica chains play: the shorter the silica chains, the lower the elastic properties. The evolution is non-linear. The major improvement arises from the dimer-to-pentamer transition due to the incorporation of bridging tetrahedrons. They, also scaled up their data in order to take into account the cement paste porosity using both the Mori-Tanaka (MT) and the self-consistent model (SC) micromechanical models [76]. They considered two packing densities (η) corresponding to high-density C-S-H gels (HD-C-S-H; $\eta \sim 0.74$) and low-density C-S-H gels (LD-C-S-H; $\eta \sim 0.64$). The obtained indentation moduli ($M = E/(1 - \nu^2)$) on the fully-dense phase combined with MT or SC approaches gave results in good agreement with experiments [85].

In 2009, Pellenq et al. [81] developed their C-S-H molecular model and computed its elastic properties. Those values are reported in Table 1 as Ref. 81. The slightly higher values than those computed for tobermorite crystals [76,127] were attributed to a more disorder and denser structure. Pellenq et al. also computed for the first time properties beyond ideal elasticity: the rupture strength, which was reported to be ~3 GPa, and the indentation modulus. For the bulk C-S-H solid, they found m_s=65 GPa, and they upscaled to that of the porous C-S-H phase (M) through the relation $M = m_s \cdot (2\eta - 1)$ [132]. Applying the previous relation, they found indentation moduli of 31.2 and 18.2 GPa for HD-C-S-H and LD-C-S-H, respectively, which is in good agreement with experiments [85].

Later, Shahsavari et al. [94] benchmarked the available force fields (at the time) for the C-S-H (i.e., the core-shell force field and ClayFF) with quantum chemistry computations of elastic properties as a reference [127]. They found that the core-shell model predicted well elastic properties, while ClayFF underestimated them [94]. Then, they used the calculated elastic constant to develop a computationally efficient force field (CSH-FF) on the basis of ClayFF [72]. The new force field reproduced the elastic properties in good agreement with data from quantum chemistry and the core-shell model, but with significantly less computational effort. Elastic properties computed with CSH-FF were reported in Table 1 as Ref. [94].

Bonnaud et al. [132] studied the effect of temperature on mechanical properties of the C-S-H phase, again using the defective molecular structure of C-S-H developed by Pellenq et al. [81]. Within a single grain, they observed increasing elastic moduli (K, G, and E) with temperature. They related this behavior to the water loss, which increases cohesion within a grain (i.e., less water reduces its screening effect). Bonnaud et al. also computed composite indentation moduli for LD-C-S-H (M_{LD}) and HD-C-S-H (M_{HD}). While most of the predicted M_{HD} values exceeded experimental values, good agreement was observed for M_{LD}. They attributed the observed discrepancy to (i) their assumption that change in packing density is only due to grain shrinkage with temperature (no grain rearrangement)cand (ii) the single-grain model that is not able to solely capture the effect of the porous network on mechanical properties [132].

In 2014, Abdolhosseini Qomi et al. [87] studied the effect of the Ca/

Table 1
Selected values of the bulk modulus (K), shear modulus (G), Young's modulus (E), and Poisson's ratio (ν) of fully dense cement phases. m_s is the indentation modulus of a single particle of C-S-H.

Phase	Ca/Si	Source	Ref.	K [GPa]	G [GPa]	E [GPa]	m_s [GPa]	ν
T. 1.1 nm	0.67	Sim.	[127]	66.65	32.03	82.82	90.59	0.29
T. 1.1 nm[a]	0.67–1	Sim.	[127]	52.7–60.8	29.8–36	75.2–90.1	80.8–96.3	0.25–0.26
T. 1.1 nm	1.0	Sim.	[94]	53.6	37.7	91.62	96.06	0.22
T. 1.4 nm	0.83	Sim.	[127]	35.91	20.61	51.90	55.64	0.26
T. 1.4 nm	0.83–1.5	Sim.	[76]	25–47.8	14–19.1	35.6–49.9	38.5–55.4	0.24–0.33
T. 1.4 nm	0.83	Sim.	[94]	42.4	19.2	50.05	55.12	0.30
T. 1.4 nm	0.83	Sim.	[128]	44.2	21.8	56.2	61.3	0.29
T. 1.4 nm	0.83	Exp.	[129]	474	–	–	–	–
C-S-H gel	1.65	Sim.	[81]	49	23	55–68	65	0.3
C-S-H gel	1.65	Sim.	[94]	50.5	21.69	56.92	63.07	0.31
C-S-H gel	1.65	Sim.	[128]	48.3	24.8	63.6	69	0.28
C-S-H gel	0.7–2.3	Exp.	[31,85,130]	18	9.7	19–28	–	0.25
C-S-H gel	0.8	Exp.	[131]	58.3	–	–	–	–
C-S-H gel	1.0	Exp.	[131]	69.7	–	–	–	–
C-S-H gel	1.3	Exp.	[131]	77.2	–	–	–	–

[a] Hamid's tobermorite.

Si ratio on mechanical properties using the extension and generalization of the C-S-H model by Pellenq et al. [81]. As experimentally found, they observed a degradation of the indentation modulus of the fully dense C-S-H phase (within a grain) with the rise of the Ca/Si ratio, because of molecular structures that become more and more defective reducing stiffness and anisotropy. Hardness exhibited a similar trend. Looking at the indentation modulus-to-hardness ratio, they found a maximum at Ca/Si = 1.5, meaning that at that particular chemistry the C-S-H phase has the lowest elastic strain limit.

Later, Hou et al. [133] continued their study on mechanical properties of the C-S-H phase by considering the effect of water attack under tensile stress. This work aimed to simulate water invasion and reaction with the C-S-H molecular structure under stress [133]. They employed, as previously, ReaxFF and Pellenq-type building scheme, but started with a C-S-H molecular structure having a ratio Ca/Si = 1.1. They generated molecular configurations under various stresses that were later equilibrated in grand canonical Monte Carlo to adjust the water content. They applied molecular dynamics again in the canonical ensemble to let the molecules react with the C-S-H solid phase. From this approach, they found a strain threshold below which water does not enter the C-S-H molecular structure. It corresponds to the elastic regime. Beyond that threshold, the higher the strain, the higher the water content. Under strain, some cavities are created within which water can adsorb. In the vicinity of silica chains containing broken bonds, confined water molecules may react with them to form hydroxyl groups (water dissociation) [133].

Shear strength has been also explored in detail, aiming to understand creep in cementitious materials. In 2013, Manzano et al. [128] compared the mechanical properties under shear strain of tobermorite 1.4 nm and the original structure of Pellenq et al. [81]. They suggested that water plays a key role in the mechanical response (i.e., yield strength, build up of pressure during shear deformations, and stress drop magnitude at large strains) of those phases. Strain is preferentially localized in water-rich regions under shear stress, which was attributed to the screening by water of strong Coulomb interactions between C-S-H sheets. Their results highlighted the fact that water acts as a lubricant in sliding motions among C-S-H nanoparticles in agreement with existing theories on creep and drying shrinkage of cement [134–136]. Palkovic et al. [137], performed a similar study with the same phase and force field, but with different shear deformation methods: a Generalized Stacking Fault method and an affine loading method. They found similar mechanisms and yield stresses independently of the method, and consistent with previous simulations [128]. The maximum shear stress is around 3 GPa, when the C-S-H layers slide over each other. Morshedifard et al. [138] introduced yet another methodology to study creep. They applied the incremental stress marching technique to ease the system in low-lying minima and allowing reaching states necessitating usually excessively long-lasting MD simulations. They used a Pellenq-like C-S-H model having a shear modulus of 21.1 ± 2.1 GPa in good agreement with previous simulation results (21 GPa [128]). They applied cyclic loading with different mean stress levels, and pointed out the role of the water content in the interlayer space of the C-S-H phase. When increasing the interlayer content, they observed a transition from viscoelastic to logarithmic creep. Due to simulation time limitations and the use of non-reactive force fields, Morshedifard et al. [138] were only able to study nonaging creep.

Bauchy et al. reported in 2015 [139] calculations on fracture toughness, critical energy release rate, and surface energy of C-S-H grains based on molecular simulations with a reactive force field (ReaxFF). Following Pellenq's approach [81], they generated a molecular model of C-S-H with a Ca/Si ratio of 1.71 from an initial tobermorite 1.1 nm crystal structure. They applied a rising tensile strain in the direction perpendicular to the C-S-H sheets and monitored the stress until complete fracture. From the external work applied on the molecular structure, they computed an average critical energy release rate G_c=1.72 ± 0.29 J/m^2. G_c is related to the fracture toughness K_{Ic} through the Irwin formula, $G_c = H_I {K_{Ic}}^2$, where:

$$H_I = \frac{1}{2}\sqrt{\frac{C_{11}}{C_{11}C_{33} - C_{13}^2}\left(\frac{1}{C_{44}} + \frac{2}{C_{13} + \sqrt{C_{11}C_{33}}}\right)} \quad (2)$$

for transversely isotropic materials with C_{ij} being the elastic constant in the Voigt notation [139]. The obtained fracture toughness was K_{Ic}=0.369 ± 0.030 MPa·m$^{1/2}$. During the fracturing process, they observed the dissociation of some free water molecules stabilizing the newly created surfaces and reducing the surface energy.

From a mechanical point of view, cement and the C-S-H phase can be viewed as an assembly of grains [140,141]. In real cement samples, fracture processes are likely to take place at the interface between grains rather than within them. Therefore knowing the cohesive forces among those grains that are at the origin of the microstructure formation and how they are affected by the environment is relevant to better understand the mechanical behavior of those materials. As a first step, Bonnaud et al. studied successively the effect of the relative humidity [142] and the temperature [132] on the cohesion between grains separated by up to 1 nm using computed pore pressures. At room temperature, they highlighted the role of calcium ions on the intragranular cohesion as well as the disjoining behavior of water. They observed a disjoining behavior of water for intergranular distances shorter than 0.5 nm, while they observed a cohesive behavior between 0.5 and 1. Calcium counterions exhibit a cohesive behavior on the whole range of studied intergranular distances. Regarding temperature, they found a maximum

of cohesion (or a minimum of pore pressure) at the onset temperature of water released from nanopores (water loss). This cohesion maximum is in good agreement with the maximum compressive strength [143] and the maximum of hardness [144] observed experimentally.

In 2016, Bonnaud et al. [145] used the defective model [81] to create particles of size ~5 nm and assess the effect of particle orientation on forces. They performed their simulation for a relative humidity of 10%, and computed mechanical properties from mean force profiles between C-S-H particles. They found (i) adhesion forces in the range 9.31-11.59 $\times 10^8$ N/m^2 that were closed to experiments (9.28 $\times 10^8$ N/m^2 [146]); (ii) Young's moduli in the range 42.28-70.69 GPa, which are close to previous simulation results for fully dense C-S-H (see Table 1); and (iii) rupture strains (~1.79-4.17%) in fair agreement with previous simulation results on the fully dense phase [81]. From a qualitative point of view, they reported that cohesion between particles is strongly affected by both the aspect ratio and the crystallographic misorientation of interacting particles and that the most stable particle pairs were those formed by identical particles with the same orientation.

In 2017, Masoumi et al. [147] have reported further data related to forces and interaction potentials between grains. In their study, they considered particles surrounded by liquid water. They employed the free energy perturbation (FEP) theory to derive the potential of mean force (interaction potentials). They used Hamid's structure of tobermorite 1.1 nm (Ca/Si = 1) and the CSH-FF in their molecular dynamics simulations [147]. They found for distances close enough an anisotropic sliding behavior mainly attributed to the orientation of silica chains at the surface of their grains. They related previous data to some mechanical properties like surface energy, cohesive pressure, and elastic properties. They found a Young modulus (77.6 GPa), a cohesive pressure (6.5 GPa), a surface energy (0.67 J/m^2), and a shear modulus (45.5 GPa) in good agreement with experimental values. In 2019, Masoumi et al. [148] deepened their study by considering finite-size particles in the layer direction and varying Ca/Si ratios from 1.1 to 1.9. For Ca/Si < 1.5, PMFs exhibit a single, primary minimum, while for Ca/Si > 1.5, they observed an oscillatory trend in PMFs. They attributed the effect of the Ca/Si ratio on the PMF behavior to a transition from a crystal structure to a glassy one when increasing Ca/Si. For molecular models having chemical compositions in the range 1.1≤ Ca/Si ≤1.9, they derived from PMFs some mechanical properties like Young's moduli (26.15-102.43 GPa), cohesive pressures (0.9-3.7 GPa), and surface energies (0.1065-3473 J/m^2) [148].

5.3. Nanoconfined water

Over the last decade, molecular modeling and simulations were proven very useful in better understanding nanoconfined water behavior in the “fully dense” or bulk C-S-H phase. The results have been discussed in the context of processes like creep and shrinkage, diffusivity, freeze-thaw, etc., and are therefore intimately ligated to the mechanical properties and the ion diffusivity.

For the interlayer space (≲1 nm) Youssef et al. [149] computed the water structure and dynamics on the defective model from Pellenq et al. [81]. In such strong hydrophilic confinement, the interlayer water (i.e., water in the ~0.5 nm space between C-S-H layers) adopts a glassy behavior at room temperature. This strong reduction of the water structure and dynamics was later observed by Ji et al. [150] and Li et al. [151] for various classical interaction potentials of water. A further investigation by these authors [128], where they used the same simulation techniques as in Ref. [91], pointed out the role of water as a lubricant in such interlayer space under shear deformations, relating this effect to C-S-H long-term relaxation in creep. Morshedifard et al. [138] observed that the amount of water in “fully dense” C-S-H is responsible for a transition from viscoelastic to logarithmic creep of the time-dependent response of the phase. Abdolhosseini Qomi et al. [87] generated various molecular structures having different chemical compositions and validated them against experiments. They showed that variations in the Ca/Si ratio (i.e., the substrate chemistry) affect water structural properties like the bond length, the dipole moment, the water density, and the average number of hydrogen bonds, and water dynamics in the interlayer space is nearly two-dimensional and close to supercooled liquids and glassy phases [152].

Beyond the interlayer space (1 nm), the C-S-H phase exhibits a gel porosity with widths between 1-10 nm [153]. A common methodology to simulate these pores is by the so-called “slit pore models”, as explained in the previous section, see Fig. 6. Bonnaud et al. [132,142,154] investigated the lower bound (1 nm) for various relative humidities (RH) and temperatures. At room temperature, they showed that cohesion between C-S-H particles was mainly driven by calcium ions, and water screens the interactions. Hence, the higher the relative humidity (i.e., the higher the water content), the less cohesive the material [142]. When increasing the temperature, they observed a water loss from the interparticle space between 373 and 473 K [132], in the line of experiments [155]. Upon temperature driven water desorption, C-S-H particles densify due to shrinkage, inducing an increase in the mechanical properties in fair agreement with experimental works [144]. Computed pore pressures between C-S-H particles exhibited a transition temperature (~385 K) below which cohesion was increased in the material and above which cohesion was decreased. This result is in qualitative agreement with experimental data like the maximum hardness [144] (~473K) and the maximum macroscale compressive strength [143] (~473-573 K). Bonnaud et al. also found transitions in properties like potential energies and the mass density of water at low and intermediate temperatures, related to the liquid-liquid transition (180-195 K) and the liquid-liquid transition (180-195 K), respectively [159]. The analysis of the translational mean square displacements revealed a glass transition temperature at around ~170 K. Above this simulated glass transition, they observed activation energies (27-41 kJ/mol) in the Arrhenius regime, i.e., for temperatures lower than 180-195 K, in good agreement with recent experiments (~41 kJ/mol) [169,170].

Properties of confined water located in the upper range of gel pores were investigated by Hou et al. [160,161]. The authors considered saturated gel pores of widths ~4.5 and 6 nm. For the solid substrate, they considered a Pellenq-like model of C-S-H. Whereas in the vicinity of the interfaces they found low diffusion rates for water, molecules recover their bulk properties (mass density, self-diffusivity) in the middle of a pore of width 4.5 [160,161]. They attributed this slowing down to the formation of hydrogen bonds between water molecules and oxygen atoms from the silica chains and to the presence of calcium ions close to the pore surface (i.e., hydration shell around calcium ions). This result is in good agreement with the findings of Duque-Redondo et al., which computed the water self-diffusion coefficient as a function of the distances from the surface for a C-S-H [156]. They obtained a similar trend in the self-diffusion coefficients, increasing up to the bulk value at the center of 5 nm pores, see Fig. 6.

Recently, Honorio and Abahri [171] studied the water flow in nanoporous tobermorite 1.1 nm molecular models, used as an analog of the C-S-H, considering pores of widths 0.8, 4.2, and 8 nm. Using Non-Equilibrium Molecular Dynamics, where a constant force was applied on fluid species in the plane parallel to the pore surface, they observed a Poiseuille flow in pores larger than 4 nm. Under a Poiseuille flow, they found similar velocity profiles for the two directions parallel to the pore surface, meaning that the atomic roughness of tobermorite does not affect significantly the water flow. The Poiseuille flow was successfully described with a slip length of ~0.265 nm. Those results demonstrate that the Navier-Stokes equation holds for a large number of mesopores (i.e., from pores greater than 4 nm up to 50 nm).

5.4. Ion diffusion in the C-S-H gel

Ionic transport in C-S-H gel is a key factor in the durability and overall performance of cement and concrete. Many authors have focused on the diffusion of chloride ions and their interaction with the C-S-H

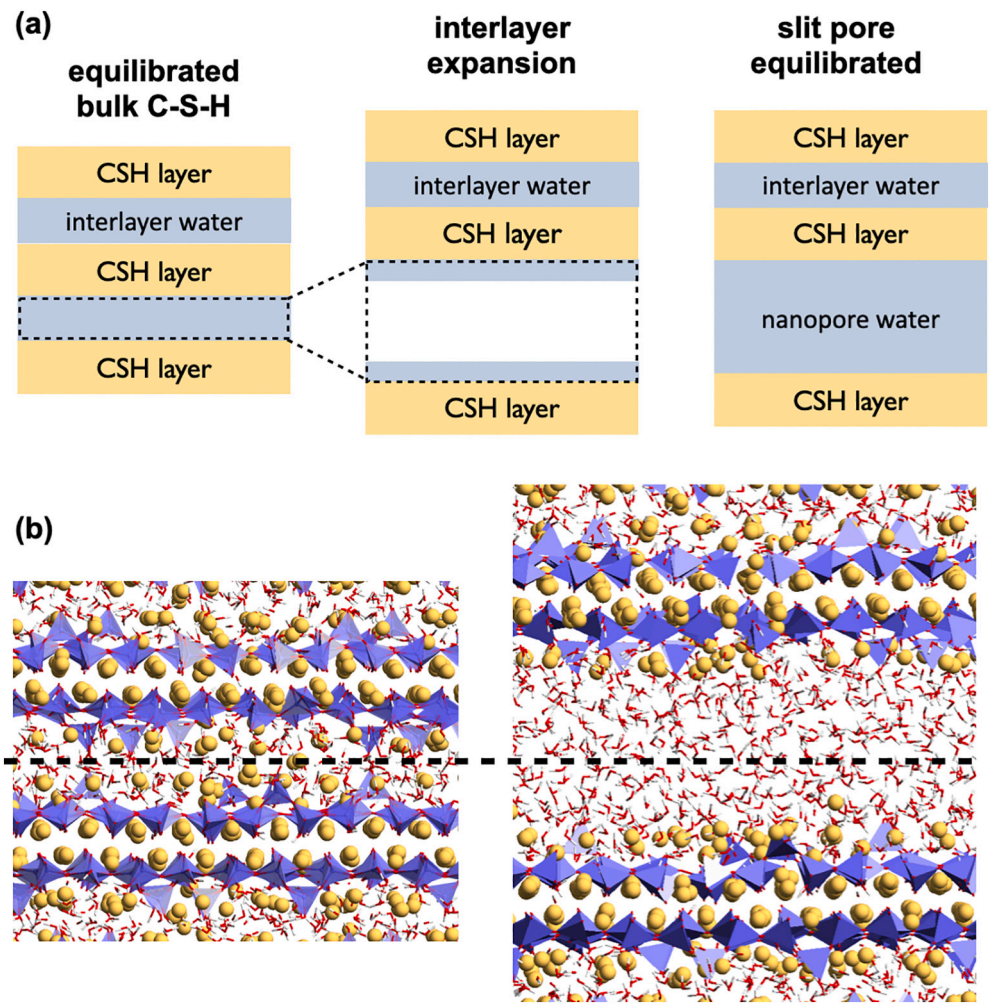

Fig. 6. (a) a) Schematic procedure for building a nanopore from a bulk C-S-H model: an interlayer space is expanded in perpendicular to the C-S-H layers, and saturated with water molecules (b) Example of an equilibrated bulk C-S-H model (left) and equilibrated C-S-H model with a slit pore created by the interlayer expansion (right).

surface as these ions are responsible for the degradation of reinforced concrete due to the corrosion of the steel bars. Ionic transport has also been studied in the context of radionuclide immobilization in concrete. It must be taken into account that the diffusivity values computed by atomistic simulation correspond to nanopores with diameters between 1 and 6 nm. A direct link with real scale diffusivity is not straightforward, as it will depend largely on microscopic and even macroscopic factors such as pore size distribution, tortuosity, presence of additional phases, chemical potential, etc. Atomistic simulations must be seen as a complementary technique to access the smallest possible scale and discriminate between the diffusion on nanopores and larger scales.

Kalinichev et al. [71] were pioneers of the molecular simulation work on interfaces between cement phases and aqueous solutions with chlorides. In their work, they provide insights on the structural and dynamical behavior of Cl^-, Na^+, and Cs^+ ions confined in nanopores of portlandite, ettringite, and tobermorite 0.9 nm, used as a model for C-S-H. The authors distinguished three types of species in the aqueous phase (see Fig. 8:

- inner-sphere surface complexes that refer to ions coordinated with atoms belonging to the solid surface;
- outer-sphere surface complexes corresponding to ions separated from the solid surface by a molecular layer;
- solvated ions in the diffuse layer or in the core of the pore (bulk) that are separated from the surface by more than one layer of water molecules.

They found that the cations (i.e., Na^+ and Cs^+) are attracted by the solid surface, but they did not observe inner-sphere Cl^- ions in the vicinity of tobermorite surfaces. Kalinichev et al. suggested that the sorption capacity for Cl^- ions of C-S-H gel can be even lower since in tobermorite the silica chains are saturated with hydrogen atoms, while in a more realistic calcium silicate hydrate phase they are less saturated (deprotonation) because of the higher pH and Ca/Si ratios, which may cause repulsive forces between the surface and the Cl^- ions [71].

Subsequent simulation studies [149,151–155,163,172] reached similar conclusions despite the differences in the models and simulation schemes (see Table 2). Basically, these studies concluded that Cl^- ions are weakly adsorbed by the surface due to repulsive interactions [149–151,153,172]. However, they highlighted that the presence of cations strongly adsorbed at the pore surfaces (inner-sphere surface complexes) facilitates the adsorption of Cl^- ions (outer-sphere surface complexes) by forming stable ionic pairs [151,153], in line with experimental studies [173,174]. Liu et al. [163] also suggest that the Ca/Si ratio strongly affects the adsorption of chloride ions at pore surfaces. They found that the chloride adsorption in C-S-H is maximum at a Ca/Si ratio of 1.2, coinciding with the maximum adsorption of cations in this work and other experimental and simulated studies [158,175,176]. The

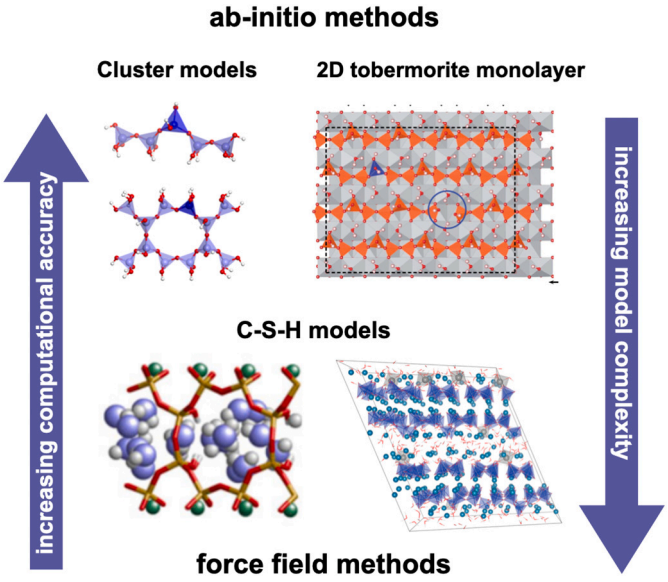

Fig. 7. Different models used to investigate Al incorporation into the C-S-H gel. The increasing complexity and size from very simple clusters to more realistic C-S-H models implies a change in the computational methodology from ab initio methods to force field methods. Above, cluster models with isolated *dreierketten* aluminosilicate chains and double chains are shown. Cluster models are used in [114,115]. In the upper right-hand corner, a 2D defective tobermorite monolayer is shown, adapted from Ref [116], with permission from The Royal Society of Chemistry. Below, detail of the C-A-S-H model with Q^3 sites from [117] is represented, reprinted with permission from The American Ceramic Society, brick C-A-S-H model from [98] accessible by https://pubs.acs.org/doi/10.1021/jacs.0c02988, with permission from American Chemical Society. Further permissions related to this figure excerpted should be directed to the ACS.

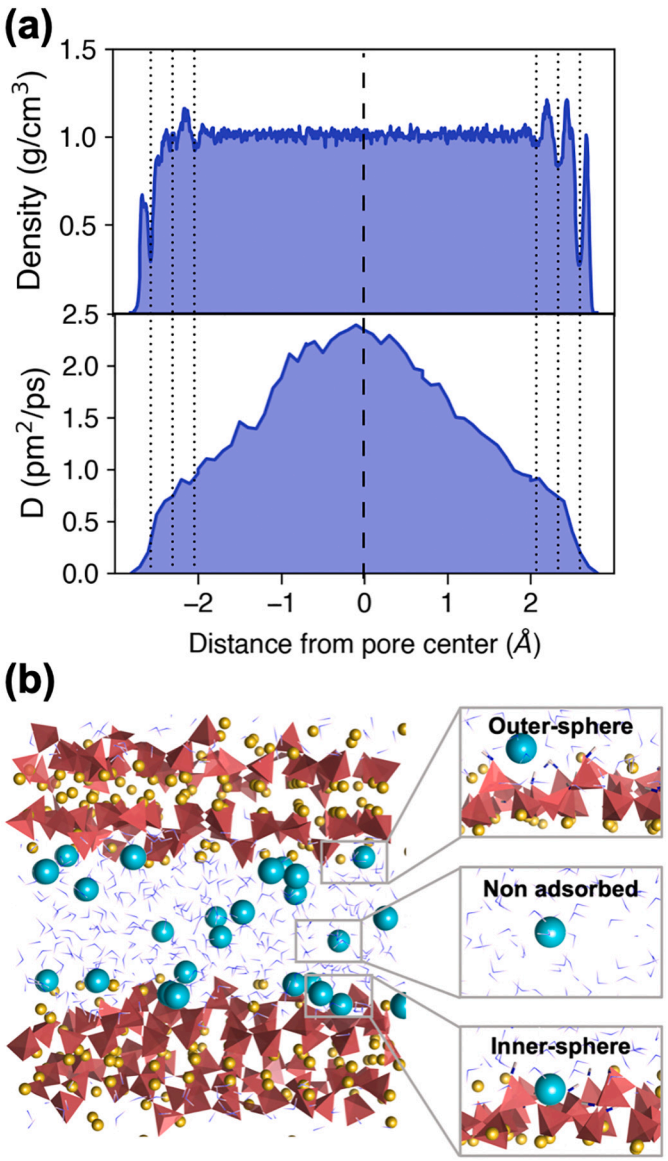

Fig. 8. (a) Atomic density profile (above) and diffusivity profile (below) for water along a 5 nm C-S-H pore [165]. (b) Cs confined in a 5 nm C-S-H pore. Insets show Cs ions in different sorption configurations. Adapted from [166] with permission from The Royal Society of Chemistry.

self-diffusivity values of chloride ions from different studies are scattered due to the differences in the models, pore sizes, ionic pairs, concentrations, and force fields, the values of chloride's diffusion coefficients cannot be directly compared. (see Table 2). For instance, Zethab et al. [152] found self-diffusion coefficients for chloride ions of $\sim 0.71\times10^{-9}$ m^2/s, on the same order of magnitude as the one derived from a collection of experimental results ($\sim 0.11\times10^{-9}$ m^2/s [177]), irrespective of the nature of the cation of the ionic pair (NaCl and $CaCl_2$). In contrast, Liu et al. found lower diffusion coefficients for Cl^- ions for $CaCl_2$ and $BaCl_2$ ionic pairs than for NaCl and KCl solutions [163]. These contradictory results of the diffusion coefficients for Cl^- ions observed in those works may be due to the concertation effect. Indeed, Wang et al. [154] showed that the higher the concentration of the ionic species, the lower the diffusion coefficients for Cl^-. Other factors can also affect the diffusion of chloride ions. For instance, Hou et al. [155] showed that the mobility of NaCl ionic pairs is slowed down in presence of sulfates. They attributed it to the immobilization of the sulfate ions by the C-S-H substrate due to the formation of strong interactions with surface Ca^{2+} ions and the ability of the adsorbed sulfate ions to capture sodium ions from the gel pore solution.

The diffusivity of cations has also been investigated by means of molecular dynamics simulations, as shown in Table 2. Pan et al. [149] found that the diffusion coefficients of Na ions in the closer domain to the surface (assimilable to inner-sphere surface complexes) were one order of magnitude lower than those located at distances of ~0.1 nm from the surface. Similar results were also found by Duque-Redondo and coworkers [156–158,172,178]. They found that the self-diffusivity of adsorbed Cs^+, Ca^{2+}, and Na^+ ions is up to two orders of magnitude lower than ions located in the core of the pore. The time autocorrelation functions showed that inner-sphere surface complexes exhibit longer residence times than outer-sphere species, which is consistent with the fact that the former ions are more strongly adsorbed than the latter, but also that the lifetime of the bonds between oxygen atoms of the silicate chains in the C-S-H and Cs^+ ions is much smaller than with Na^+ and Ca^{2+} ions due to the smaller ionic radius and/or the higher partial charge carried by the latter ions. This is in agreement with the findings reported by Jiang et al. [150], who indicated that the smaller hydration shells of the Na^+, and K^+ ions regarding Cs^+ ions facilitate their penetration into surface cavities and the formation of stronger bonds with oxygen atoms of silicate chains, which significantly slow down their dynamics: $D_{Na}<D_K<D_{Cs}$. Furthermore, Duque-Redondo et al. analyzed the role of Ca/Si and Si/Al ratios on the dynamics of the Cs^+, Ca^{2+}, and Na^+, as well as the effect of the counterion (Cl^-, OH^- or SO_4^{2-}) [172]. The higher the Ca/Si and Si/Al ratios, the higher the amount of Cs^+ ions in the core of the pore (desorbed, solvated ions) due to the reduction of adsorption sites on the C-S-H substrates with respect to those with low Ca/Si and Si/Al ratios [156,158,178]. The sulfate ions can form $CaSO_4$ ionic pairs and remove Ca^{2+} from the C-S-H surface, increasing the adsorption of other cations in the adsorption sites occupied by those Ca^{2+} ions. Hou et al.

Table 2
Table summarizing diffusion coefficients computed from Molecular Dynamics simulations applied on various molecular structures for the substrate including Tobermorite, C-S-H, and C-A-S-H gel. C, 1 L, 2 L, S, and I stand for the core of the pore, the first adsorbed layer, the second adsorbed layer, the surface, and the interlayer. In the force field section, FF1, FF2, FF3, FF4, and FF5 stand for ClayFF, COMPASS, CSHFF, ReaxFF and Åqvist parameters, respectively.

Tobermorite																	
Ca/Si	Ref.	Force Field	T [K]	Pore		Concentration [M]						$D \times 10^{-9}$ [m^2/s]					
				Loc.	∅ [nm]	Ca^{2+}	Na^{+}	K^{+}	Cs^{+}	Cl^{-}	SO_4^{2-}	H_2O	Ca^{2+}	Na^{+}	K^{+}	Cs^{+}	Cl^{-}
0.83	[149]	In ref.	298	1 L	2.5	–	0.3	–	–	0.3	–	–	–	0.083	–	–	–
				2 L								–	–	0.352	–	–	–
				C								–	–	0.802	–	–	2.334
1	[150]	FF1	300	1 L	4.5	–	–	–	–	–	–	~0.2	–	–	–	–	–
				2 L		–	–	–	–	–	–	~1.0	–	–	–	–	–
				C		–	–	–	–	–	–	~2.0	–	–	–	–	–
				C		–	0.5	–	–	0.5	–	1.72	–	0.71	–	–	–
				C		–	–	0.5	–	0.5	–	1.71	–	–	0.93	–	–
				C		–	–	–	0.5	0.5	–	1.80	–	–	–	1.25	–
1	[151]	FF1	300	1 L	4.5	–	0.44	–	–	0.44	–	~1.0	–	–	–	–	0.24–0.48
				2 L								~2.9	–	–	–	–	0.67–1.16
				C								3.9–4.3	–	–	–	–	2.15–2.36
1	[152]	FF2	300	C	6	–	0.56	–	–	0.56	–	1.14	–	–	–	–	0.6643
						0.28	–	–	–	0.56	–	1.23	–	–	–	–	0.7551
0.83	[71]	FF1	298	C	4	–	–	0.25	–	0.25		–	–	–	–	–	–
0.83	[153]	FF1	300	C	6.5	0.22	–	–	–	0.44		–	0.023	–	–	–	1.73
0.83	[154]	FF1	300	C	3.2	–	–	–	0	0		2.2	–	–	–	–	–
									0.5	0.5		2.1				1.1	1.4
									1.0	1.0		2.1				0.9	1.1
									1.5	1.5		1.8				0.8	0.9
									2.0	2.0		1.8				0.7	0.7
0.83	[155]	FF1	300	C	3.5	–	1	–	–	1	–	10.2	–	–	–	–	–
							2			–	1	7.5					
							1.5			0.5	0.5	9.1					
C-S-H																	
1.1	[156]	FF1	300	C	1	5.38	–	–	–	–	–	–	~0.0006	–	–	–	–
		FF3				–	5.38	–	–	–	–	–	–	~0.004	–	–	–
		FF5				–	–	–	5.38	–	–	–	–	–	–	~0.06	–
1.1	[157]	FF3	300	C	1	–	–	–	0.2	–	–	0.19	–	–	–	0.001	–
		FF5				–	–	–	5.2	–	–	0.29	–	–	–	0.05	–
1.1	[158]	FF3	300	1 L	1.44	–	–	–	3.6	–	–	~0.15	–	–	–	~0	–
		FF5		2 L		–	–	–	3.6	–	–	~0.3	–	–	–	~0.2	–
				C		–	–	–	3.6	–	–	~0.35	–	–	–	~0.3	–
1.65	[159]	In ref.	300	C	1.48	–	–	–	–	–	–	1.15[a]	–	–	–	–	–
			190	C		–	–	–	–	–	–	0.06[a]	–	–	–	–	–
			450–575	S		–	–	–	–	–	–	~0.6[a]	–	–	–	–	–
2.0	[158]	FF3	300	1 L	1.57	–	–	–	3.5	–	–	~0	–	–	–	~0	–
				2 L		–	–	–	3.5	–	–	0.05	–	–	–	~0	–
				C		–	–	–	3.5	–	–	0.05	–	–	–	0.05	–
1.7	[160]	FF4	300	1 L	4.5	–	–	–	–	–	–	0.08	–	–	–	–	–
				2 L		–	–	–	–	–	–	0.8	–	–	–	–	–
				C		–	–	–	–	–	–	2–2.66	–	–	–	–	–
1.7	[161]	FF1	300	I	1	–	–	–	–	–	–	0.003	–	–	–	–	–
				S	6	–	–	–	–	–	–	1.2	–	–	–	–	–
				C	6	–	–	–	–	–	–	1.7–2	–	–	–	–	–
0.69	[162]	FF4	300	C	0.7	~10.5	~6.7[b]	–	–	–	–	–	Na+ > Ca2+ > Al3+ > Mg2+				
1.2	[163]	FF1	293	C	5	0.85	–	–	–	1.7	–	–	0.5	–	–	–	1.2
						–	0.85	–	–	0.85	–	–	–	1.2	–	–	1.4
						–	–	0.85	–	0.85	–	–	–	–	1.1	–	1.3
C-A-S-H																	
1.1	[156]	FF1	3*300	3*C	3*1	5.38	–	–	–	–	–	–	~0.0006	–	–	–	–
		FF3				–	5.38	–	–	–	–	–	–	~0.003	–	–	–
		FF5				–	–	–	5.38	–	–	–	–	–	–	0.028	–

[a] Mean square displacements (MSDs) computed from unconfined coordinates (2D), i.e., in planes parallel to pore surfaces (slit pores).
[b] Same concentration for Mg^{2+} and Al^{3+}.

[162] investigated the mobility in the interlayer of Ca^{2+}, Mg^{2+}, Al^{3+}, and Na^{+} ions using ReaxFF. They found residence times for water in the hydration shell of Al^{3+} and Mg^{2+} ions much greater than the ones for Na^{+} and Ca^{2+} ions and diffusion coefficients that follow the order: $D_{Na}>D_{Ca}>D_{Al}>D_{Mg}$. Nevertheless, the results from this paper should be taken with care, since the ReaxFF parameters for Mg, Al, and Na in combination with the Ca/Si/O/H set have not been tested properly.

5.5. C-S-H hybrids and composites

In pursuit of developing more sustainable building materials and their use in innovative applications, a wide variety of additives or chemical admixtures have been used. [179–185]. The intercalation of organic molecules or low dimensional materials into the C-S-H gel at the nanoscale could have a synergistic effect that results in enhanced performance of the hybrid C-S-H or composite material [186–192]. Atomistic simulations are an excellent tool to provide detailed information about the nanoscale interaction between the C-S-H gel and the different additives. As a matter of fact, MD simulations have already been used to investigate the organic-inorganic interactions in other layered materials, like clays [101,102,107,193–196] and layered double hydroxides [197].

In 2008, Sanchez and Zhang were pioneers in the atomistic modeling of C-S-H composites [193]. They studied the interfacial interactions between C-S-H, using as a model the structure of tobermorite 0.9 nm [198], with graphite and graphite functionalized with hydroxyls, carboxyl, carboxylate, carbonyl, and amine groups. They found that the binding affinity of the graphitic structures to the surface of tobermorite increases with the polarity of the functional group, enhancing the stability of the interphase and the overall strength and durability of the resulting composite. Subsequent MD studies using Pellenq-type models confirmed the significant improvement in Young's modulus and strength for functionalized graphene/C-S-H composites and, to a much lesser extent, in non-funcionalized/C-S-H composites regarding pure C-S-H [199–201]. These studies also reported that higher Ca/Si ratios may contribute to increase the tensile strength due to the formation of more Ca—O ionic bonds between the Ca ions of the C-S-H and oxygen atoms from the graphene oxides (GO) [201].

Atomistic modeling was used to study the mechanical properties of C-S-H reinforced with carbon nanotubes (CNT) inserted along the weakest direction, perpendicular to the C-S-H sheets [202]. The authors reported an increase in the ductility and significantly higher tensile strength in the perpendicular direction of silicate layers, while the compressive behavior was not substantively altered. However, they found a worsening of the shear strength in all directions for the C-S-H/CNT composites. More recently, the use of different surfactants to disperse the CNTs into the cement matrix was also investigated [203]. Based on the interactions between CNTs and the dispersing agents in bulk water, the Gum Arabic (GA) was identified as the most suitable surfactant since only GA was able to interact with both the CNTs and the C-S-H surface. The mechanical characterization revealed that the incorporation of the CNT along with GA in a drilled hole perpendicular to the silicate chains doubles the overall strength, increases considerably the elastic, shear, and bulk moduli, and switches the nature of the material from brittle to ductile.

Besides graphene and CNTs, other organic compounds have been used to improve the mechanical performance of the C-S-H gel (Fig. 9). Hou et al. investigated the intercalation of poly(acrylic acid) (PAA), poly (vinyl alcohol) (PVA), and poly(ethylene glycol) (PEG) in the interlayer space of a C-S-H model with a Ca/Si ratio of 1.3 [204–207]. They used different force fields with different results. When they used a combination of ClayFF [72] or CSH-FF [94] with CVFF [208], they observed an increase in Young's modulus, tensile strength, and failure strain, while improving the ductility. In contrast, the polymer intercalation barely affected the Young's modulus and tensile strength when ReaxFF is used [207]. The authors attributed these differences to the rupture of C—C bonds from the polymers to form C-O-Si. However, this unrealistic result can be due to a methodological flaw since the ReaxFF Ca/Si/OH set of elements is incompatible with organic parameters. In any case, further research is needed to evaluate the quality of the different FFs.

The elastic response of C-S-H/PEG composites was also studied by Zhou and coworkers comparing simulations and experiments [209]. Experimental HP-XRD measurements revealed a significant increase in the bulk modulus of the C-S-H/PEG composite (K = 52.7 GPa) with respect to a pure C-S-H sample (K = 45.6 GPa). MD simulations reproduced the pure C-S-H value (K = 45.9 GPa), yet predicted a considerable decrease for the C-S-H/PEG composite (K = 34.7 GPa). The authors suggested that in the experimental samples, PEG is located in large pores within C-S-H particles and not sandwiched in the interlayer space as was assumed for the simulation model. The result points out the importance of a correct model.

Continuing with polymers and organic molecules, a variety of studies have investigated the adhesion or adsorption and the interaction of organic moieties with C-S-H substrates. Overall, the results show the same qualitative results: highly-polar polymers, with carboxyl and

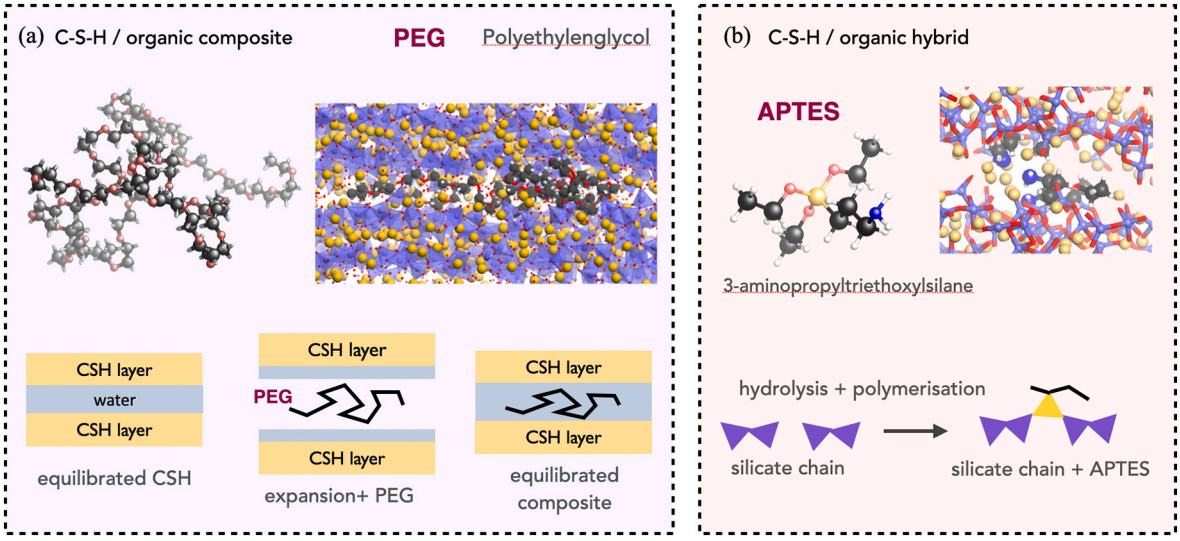

Fig. 9. Two examples of C-S-H organic interactions. (a) C-S-H/PEG composite. A PEG chain of 40 monomers is inserted into the C-S-H interlayer space. (b)C-S-H/APTES hybrid. The APTES forms covalent bonding with the C-S-H silicate chains.

amide groups, adsorb better in C-S-H as the Ca/Si ratio increases due to the interaction with Ca and formation of hydrogen bonds [210–212]. On the contrary, low adhesion energies were reported for polymers like polypropylene, which does not have polar groups on its structure.

Polymers are also used to improve the adhesion between the C-S-H surface and other phases. For instance, Han et al. used PVA to enhance the adhesion of rubber hydrocarbon (RH) to the C-S-H [213]. According to their calculations, the adhesion energies of the PVA/C-S-H and RH/PVA interfaces were much higher than that of the RH/C-S-H interface, suggesting that PVA is a good candidate as a bridge between the RH and the C-S-H. Thus, the presence of PVA enhances their adhesiveness and mechanical performance or rubberize cements, in agreement with the experiments, which show a significant increase in the adhesive and compressive strength for RH/PVA/C-S-H composites. Sulfur-black carbon (SBC) polymers have been used to improve the poor adhesion of concrete layers created with concrete 3D printing technology. Hosseini et al. created CSH-SBC-CSH models by sandwiching SBC polymers between C-S-H gel layers and subjected the composite to shear and tensile strains to analyze the mechanical performance [214]. The simulations show that the formation of electrostatic interactions between the SBC polymers and the Ca ions from the C-S-H surface increase the interfacial shear and tensile strengths of 50% and 88% regarding the pristine C-S-H, in the line with the experimental results obtained by three-point bending loading tests. The affinity of certain organic molecules, as gluconate, for Ca ions was exploited by Androniuk, Kalinichev, et al. to enhance the uptake of uranyl ions in C-S-H at Ca/Si ratios between 0.83 and 1.4 [215,216]. They found that gluconate is not directly bound to the C-S-H, but it creates complexes with the Ca ions from the C-S-H surface. In this way, the complexation of gluconate with Ca reduces the binding strength of these cations to the C-S-H and leaves vacant sorption sites on the surface that can be occupied by uranyl, enhancing indirectly the uranyl uptake.

6. Discussion and perspectives

In this section, we will discuss several practical aspects of the current computational models, as well as future directions.

6.1. Which available C-S-H computational model is the best?

First of all, we must stress that the discussed C-S-H models belong to the same family, which could be classified as “imperfect tobermorite” models. They have differences (missing pairing sites, interlayer Ca positions, disorder degree) but the very basic foundations are the same. That said, we can classify the C-S-H model construction into two main groups: the defective-tobermorite models and the brick model [97]. The first group includes Pellenq-type models [81,87] and Kovačević's model [95], which can be seen as a specific formulation for a Ca/Si = 1.68. The original models as presented by the authors had important differences, but, in principle, one could reach the same C-S-H final structure using either construction method. It must be noted that we will discuss the construction method rather than the specific models presented in the original papers. For instance, Pellenq's original model had some structural features, such as silicate monomers, necessary to reach Ca/Si ratios > 1.5. However, the 3n-1 rule can be fulfilled by adding $Ca(OH)_2$ in the interlayer space as proposed later [87,95,97] and Ca/Si up to 2 have been reported [156].

The brick construction method [97] is an elegant solution to build a vast number of random models with the desired composition by mixing the type and position of the predefined building blocks (see Table 3). The structure of a given model is easy to track by using the bricks' codes, which make them reproducible. It is possible to do a direct computation of the C-S-H model properties from those brick codes, like the Ca/Si ratio, MCL, formal charge densities, protonation degree, etc., with little effort. In addition, having a clear alphanumeric code to define structures sets the ground for machine learning applications [217–219].

Table 3
Summary of the discussed practical aspects and differences between the defective-tobermorite and brick-based C-S-H building methodologies.

	Defective tobermorite	Brick model	Description
Usability	✓		Easy and fast to build up to 10 models without coding
Mass production	✓	✓	Capacity to build hundreds of models with a code
Rigurosity		✓	Confidence in correct chemical coordination, hydroxylation degree, charge balance...
Order/ Disorder	Disorder	Order	Degree of structural order of the initially generated structures
Transferability		✓	Possibility to reproduce the exact same model by other authors
Flexibility	✓		Possibility to create models with a wider range of compositions and structures (for instance Q^3 sites)

Furthermore, it is possible to extend the model by adding additional and/or specific bricks for C-S-H surfaces [97] or with Al for C-A-S-H [98]. As limitations of the brick model (as it has been presented so far), we could mention that the resulting structures have a considerable structural order. The interlayer species (Ca^{2+}, OH^-, and water) are positioned in similar initial positions in each block, inducing some correlation and ordering in the structures. This may not be an issue in the context of C-S-H synthesized under controlled conditions [8], but may not be a general case. To encircle this possible problem a larger collection of bricks could be defined, or the bricks could be used to build the dried skeleton and water introduced randomly with a packing algorithm. Unfortunately, a practical implementation of the brick model needs a considerable programming effort, and so far it has been used only by its developers [97,98].

The defective-tobermorite model is the one generally used by researchers. Overall, this construction method is more general, as the C-S-H model does not need to rely on predefined bricks. It is relatively simple and fast to build 1–5 different C-S-H samples for a particular study without coding, just using visualization software like CrystalMaker [220], VESTA [221], or Avogadro [222], and build C-S-H models for specific applications, broadening the studies to less common structural features. For instance, tobermorite 1.1 nm can be used to build C-A-S-H models with Q^3 sites bridging adjacent layers (not developed yet for the brick model). The construction method described in the original references [81,87] did not include any silanol or hydroxyl groups, which were formed later during a molecular dynamics simulation from the dissociation of water molecules [91]. This would result in a Si-OH + Ca-OH pair of hydroxyl groups, which is not consistent with the experimental trend [60,223]. Nevertheless, it is possible to set their number during the construction to avoid that problem. The obtained C-S-H gel structures are generally more disordered than those of the brick model, especially at high Ca/Si ratios. This is considered to be more representative of C-S-H obtained from cement or C_3S hydration, but in some cases can lead to instabilities in the models, losing their layered structure.

6.2. How do I build a defective tobermorite model?

It is relatively simple to build a defective tobermorite model following the recipes given in [81,87,157]. Tobermorite minerals are used as a bedrock for C-S-H model development. But then, which member of the family should be used to rationalize the experiments and build computational models? In principle, there is no limitation. Any of them could be a valid starting point, provided that the structural modifications needed to match the C-S-H experimental stoichiometry and structure are introduced correctly. More rigorously, the thermodynamic properties of a system in a given stable state are independent of the path followed to reach that state. As an example, we can consider a common

step in the construction scheme of the C-S-H: the removal of the interlayer water from the initial crystalline structure and reinsertion after creating defects. In the original scheme from Pellenq [81], the defective structure without water was relaxed, with the consequent shrinkage of the basal space, and then water was introduced at the fixed volume by Grand Canonical Monte Carlo. This procedure results in the "correct" water content for a given basal distance. But it is computationally expensive. Alternatively, and given that we roughly know the experimental water content [14,41], one could directly introduce the necessary amount of water molecules using a random packing algorithm [224], and then relax the volume of the system. In both cases, the final thermodynamic state should be the same, reaching the correct water density by different paths: fixing the volume and changing the number of molecules in the first case, or fixing the number of water molecules and changing the volume in the second case.

As general boundaries, the structures must fulfill Richardson's stoichiometry, the 3n-1 rule for the silicate chains, and other aspects shown in the next section. Of course, we assume that the selected computational method provides a realistic description of the chemistry, i.e. local coordination around Ca and Si, water structure, etc). Besides those points, some hints are given below:

— If high Ca/Si ratios are desired, when calcium silicate layers are independent, both tobermorite 1.4 nm and Hamid's tobermorite are good choices. Tobermorite 1.4 nm is more similar to the C-S-H in terms of water content, yet its density, 2.23 g·cm^{-3} [79], is considerably lower than the experimental one, 2.60 g·cm^{-3} [14], and the basal space too large. Hamid's tobermorite is often preferred as a starting point, as the smaller basal distance and lower water content imply a higher starting density, 2.39 g·cm^{-3} [30]. Nevertheless, after modifications to reach a given stoichiometry and silicate chain structure, both Hamid's tobermorite and tobermorite 1.4 nm should ideally converge.
— If C-S-H with the presence of Q^3 sites is desired (low Ca/Si or high aluminum contain), tobermorite 1.1 nm or clinotobermorite should be used to model C-S-H gel due to [225]. The differences between normal or anomalous tobermorite 1.1 nm, located at the interlayer space [28], should vanish after the necessary modifications to achieve disorder. In contrast, the differences between the complex modules A and B for clinotobermorite and tobermorite 1.1 nm (see Section 2) may persist when the defects are introduced. In this case, the structural differences are subtle, and the preference of one structure over the other is difficult to predict.

6.3. Model validation and prediction of C-S-H gel properties

The reader may have noticed that we have discussed the "quality" of the models without much quantitative validation or comparison with experimental data. Despite the large number of recent publications, the lack of connection between the C-S-H atomic scale modeling and the experimental properties is still an open issue in the field. The difficulty arises from the diverse time and length scales involved in computation and experiments. Most of the experimental measurements involve large sample volumes that include important heterogeneities in the composition and structure of the C-S-H gel, pores filled (or not) with a pore solution in equilibrium with the C-S-H, etc. Therefore, the link between the experimental data about the C-S-H gel and the computational atomistic models is indirect at best. However, following our current knowledge, there are several characteristics based on experiments that can be considered as a checklist for C-S-H model validation. Some reference values are given in Fig. 10:

— XRD. Any C-S-H model must be X-ray amorphous, i.e. the lack of long range crystalline order is a necessary characteristic of any C-S-H model. The exception is the (002) reflection at small angles corresponding to basal distances between adjacent layers of ~10–14 Å, indicative of the well defined layers. A realistic model should have a layered structure [16,17,60]. In addition, synchrotron XRD experiments give access to Pair Distribution Functions (PDFs) which describe the short range order of the structure [19,34]. The PDFs are collected for the whole sample, and may include features that do not correspond to the bulk. Nevertheless, a general agreement with the experimental PDFs is desirable.
— NMR measurements. From Si-NMR experiments it has been possible to quantify the mean silicate chain length as a function of the Ca/Si ratio, and the structure of those chains (*Dreierketten* arrangement and 3n-1 rule, see Section 2). A C-S-H model should in principle reflect that structure, although the silicate chain structure is still the subject of recent studies [96]. Similarly, Al-NMR data must also be observed when Al is incorporated into the models.
— IR and Raman spectroscopy. Spectroscopic techniques have been used to determine the relative concentration of silanol groups, hydroxyl groups linked to Ca, and water within the C-S-H gel [13,41,60]. As in the previous cases, the technique will give a global value for the whole sample, including surface groups and species dissolved in the pore solution. Nevertheless, the concentration of hydroxyl groups follows a significant trend with the Ca/Si ratio that should be preferably followed. The same holds for the water content within bulk C-S-H as a function of the Ca/Si ratio: despite an indirect measurement in dried sample, the values were validated by estimations from SANS [14] for Ca/Si ratios of ~1.65, and should be taken into account.
— Neutron Scattering. Small Angle Neutron Scattering (SANS) was used to investigate the composition, density, and size of C-S-H nanoparticles [14]. An important characteristic that C-S-H models must follow is the higher density compared to tobermorite crystals, between 2.5 and 2.65 g·cm^3 for the C-S-H gel compared to the ~2.2 g·cm^3 of tobermorite 14 Å [14]. This value was later on corroborated by ^{1}H-NMR relaxometry [228]. Therefore, C-S-H atomistic models would be denser than their

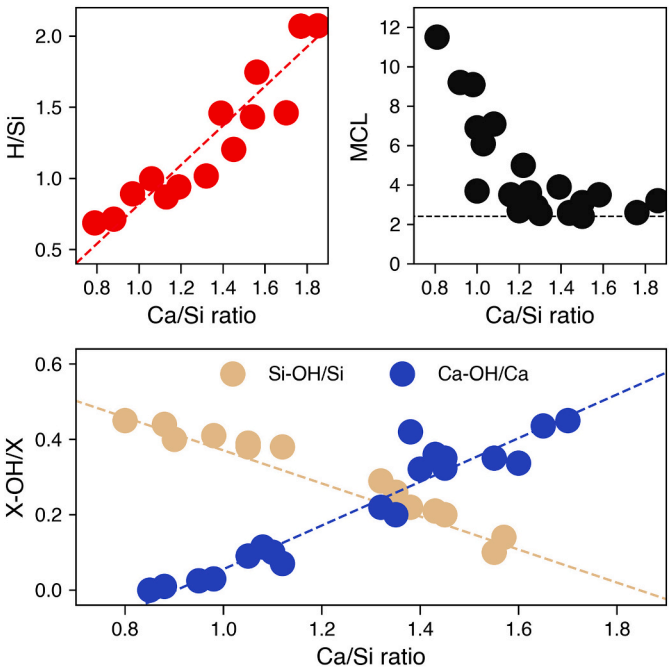

Fig. 10. (a) Silicate Mean Chain Length as a function of the Ca/Si from [8,64,87,226,227] (b) Si-OH/Si and Ca-OH/Ca ratio as a function of the Ca/Si [13,41,60,223] (c) Water to silicon ratio as a function of the Ca/Si ratio [41].

crystalline counterparts. On the other hand, Inelastic Neutron Scattering experiments have been used to quantify the Ca-OH/Ca ratio as a function of the Ca/Si ratio, being complementary to spectroscopic techniques [223].

6.4. Current problems and limitations with C-S-H computational models

First of all, it is important to make a clear distinction between what is a valid C-S-H atomistic description and what is not. A non-negligible number of publications name as C-S-H a fully crystalline tobermorite structure [229], or even a fully disordered glass without layered structure. Those systems, together with cluster models, may be used as oversimplified models to investigate very specific aspects of the C-S-H gel, but are not valid descriptions in most cases. To be labeled as "C-S-H model" the atomic structure should have finite silicate chains, higher Ca/Si ratios and density than tobermorite minerals, and certain disorder to avoid at least the long-range order characteristic of crystals.

A second concern is that nowadays atomistic simulation studies on the C-S-H are essentially irreproducible. Usually, scarce details of the building procedure are given, and the absence of an actual file in a readable format (like the Crystallographic Information File [230] or the Protein Data Bank [231]) makes it virtually impossible to reproduce an exact model. Few works include in their S.I. fully reproducible atomic structure [8,81,95,97,98]. Therefore, the standardization of the C-S-H models used for simulations is urgent. The brick model has an intrinsic advantage in this sense. The use of predefined building blocks makes it simple to identify a C-S-H gel structure based on a unique code that specifies the constituent blocks and their order. Therefore, this unique code allows two different authors to build exactly the same model. Unfortunately, the code used to combine the bricks in the original paper [97] is not available for the community nowadays. This standardization is more complex in the case of the defective-tobermorite models since their construction involves random steps, i.e. the removal of silicate groups from the silicate chains and the insertion of counterbalancing ions, Ca, hydroxyl groups, and water molecules. Therefore, they cannot be duplicated exactly. The best option for a good research reproducibility would be to collect them in a "C-S-H structure database". Existing models and new ones could be labeled with an ID number, so they could be used for reproducible purposes as well as new investigations.

In addition, we should always be aware of the variable structure of the C-S-H when we compute its properties. Even for a specific Ca/Si ratio, there is a humongous number of possible configurations, and particular models could have large deviations from the average properties. As a fast example: if we aim to build a C-S-H model made by replicating the unit cell of tobermorite 3x3x2, and then we remove just 4 out of the available 72 bridging sites, we have more than 24×10^6 possible combinations! Most of the 24 million configurations above mentioned will have the point defects homogeneously distributed along the silicate chains, resulting in similar energies. But in the particular case of the 4 defects in neighboring sites, or in the same silicate chain, the structure may be energetically unfavorable. Therefore, it is necessary to understand the sensitivity of the different properties to the particular configuration, yet most publications report properties collected for a single structure. Another interesting case was discussed by Mohamed and coworkers in [97]. They revisited the C-S-H models in the S.I. of reference [95], and they found regions with considerable charge excesses within an overall neutral system. From a statistical point of view, we could expect a considerable local charge homogeneity in the C-S-H gel, with narrow deviations, and that model would represent a conformation with less weight in the final average properties. Therefore, using results from a single C-S-H model is not correct from the statistical point of view, and a compromise between computational cost and good configurational sampling should be sought.

6.5. Practical computational hints

We have discussed the statistical validity of the results and the compromise between good sampling and computational cost, we think that it is interesting to give some practical hints. There are many different factors that may have influence both on the computational performance and on the simulation results.

Due to the typical number of atoms in C-S-H models, above a thousand in the best case scenario, the use of ab initio methods is usually prohibited. The application of these methods is limited to compute properties inaccessible to empirical potentials in small model systems, such as NMR shifts [98,234], or for benchmarking purposes [116,234,235]. Regarding empirical potentials, there are several implementations available for the atomistic simulation of C-S-H gel, being the most common ones ClayFF [72], CSH-FF [94], CementFF [233], the Interface FF [232], and ReaxFF [236]. Despite an existing review of their capabilities and limitations [237], we lack a real exhaustive benchmark of the impact of the force field choice when C-S-H properties are computed. In addition, there is a considerable number of papers that report doubtful force field choices. For instance, ReaxFF [91,236,238] is a very flexible potential capable of studying both disordered and ordered phases and is the only force field that can reproduce chemical reactions in C-S-H. But it also has some limitations, such as its high computational cost, even 40 times slower than other FF (see Table 4). More importantly, it has not been specifically parametrized for the interaction of common elements in cement like Cl, Mg, Zn, etc. with C-S-H, and, in its current form, the C-S-H potentials are incompatible with organic compounds. In contrast, IFF [232] has been specifically parametrized to be compatible with common potentials for organic compounds and should be the natural choice for hybrid systems. ClayFF [72] is also a very common choice for modeling C-S-H, compatible with organic force fields and a wide variety of aqueous ions. However, it has limitations to reproduce some of the C-S-H properties like elasticity, as it was initially developed for clay and clay-related materials. The CSH-FF [94] potential was a reparametrization of ClayFF which makes it, in theory, more suitable to reproduce C-S-H systems. On the bad side, the IFF, ClayFF, and CSH-FF use partial charges on the atoms that were developed for particular cases, usually tobermorite, and they need to be modified from the reported values to reach electroneutrality in each C-S-H model, introducing new uncertainties in the results. The CementFF solves the issue using formal charges on atoms. Despite formal charges being a less realistic representation than partial charges, they can be used consistently over a wide range of structures. In addition, the CementFF uses a core-shell or Drude polarization scheme which proves to be necessary to reproduce accurately certain properties [239]. The cost to be paid is computational

Table 4
Summary of the most employed force fields and their main characteristics.

Force field	Speed	Charge scheme	timestep (fs)	Key aspects	Ref
ClayFF	ref	Partial, fixed, non-polarizable	1	Developed for clays aqueous ions compatible with C-S-H	[72]
CSH-FF	x1	Partial, fixed, non-polarizable	1	ClayFF reparametrized for C-S-H	[94]
IFF	x1	Partial, fixed, non-polarizable	1	Special focus on compatibility with organic FFs	[232]
ERICAFF	x0.25	Formal, fixed, polarizable	0.2	C-S-H specific and polarizable	[233]
ReaxFF	x0.025	Partial, variable, polarizable	0.1	Reactive FF	[91]

performance, due to the increase in the number of particles and decrease of the integration time step. Machine learning Potentials (MLP) may be an interesting alternative in a close future. Some initial efforts have been started in the field [240,241], yet still focused on tobermorite and with a high computational cost.

The computational resources is another parameter to be considered. Some tests for illustration are given in Table 4. The simulation time strongly depends on the force field, number of atoms, number of processors, and hardware architecture. The tests were made with a C-S-H model with a Ca/Si ratio of 1.65 and w/Si ratio of 1.6. The initial system had 749 atoms, and subsequent sizes were built by replicating the simulation box, up to 13,482 atoms. The simulations were done in the supercomputer of the UPV/EHU, using Xeon 2680v4 cores at 2.8 GHz. In Fig. 11 it can be seen the different performance of the FFs, and the expected simulation times with the system size using 8 cores. Considering a simulation box of ~4.5x3x5 nm with ~6500 atoms, we can simulate per day nearly 5 ns with ClayFF, CSHFF, and IFF, 1.25 ns with ERICAFF, and 0.125 ns with ReaxFF. Longer times can be achieved by using a larger number of processors, as shown in 11. The speed up with the number of cores is not linear, and depends on the FF used. For the previous example, an increase from 8 to 32 cores will translate into ~ 12 ns/day with ClayFF, CSHFF, and IFF, 3.75 ns/day with ERICAFF, and just 0.2 ns/day with ReaxFF. Those numbers are just a guidance, as the speed up depends also on the system size and on other computational details. But the orders of magnitude are clear, and they are important for the study of some properties. There is no such a thing as an "ideal simulation time", yet the experience advises us that simulations below ns might not be properly equilibrated and are of dubious quality. Furthermore, longer simulations could be necessary for some properties. For instance, transport properties like diffusivity or viscosity, are very sensitive to the system size and to the simulation time [242], and even hundreds of ns could be necessary. Similarly, when mechanical properties are computed, the effect of the strain rate must be carefully checked to avoid unrealistic responses from the material.

6.6. *What is next? Do we need more/new/better C-S-H (computational) models?*

If we accept the consensus on Taylor's model, with a C-S-H gel made of tobermorite-like layers with defective silicate chains and additional calcium ions in the interlayer space, current computational models are enough to cover all the possible structures and stoichiometries if they are built with care. Thus, we consider that more/better models to describe tobermorite-like C-S-H are not necessary. If on the contrary, we do not assume that Taylor's model describes the C-S-H gel, or at least not all the possible varieties of the gel, we would need to build and test new models.

For instance, the C-S-H structure for low Ca/Si ratios can be easily described using Taylor's model, but high Ca/Si ratios are clearly a problem. By removing all the bridging silicate groups and compensating all the dangling siloxane groups with Ca, the maximum possible Ca/Si ratio is 1.5. In fact, recent studies based on pair distribution functions from high-energy X-ray experiments have proposed that clinotobermorite-like layers and portlandite mono- or bi-layers should coexist in the C-S-H gel [19,34], setting the Ca/Si threshold to 1.23 [34]. However, Kumar and coworkers [8] used a very fine-tuned synthetic method to obtain C-S-H with Ca/Si ratios up to 2 without detecting the presence of portlandite. The difference between those structures has great implications on the C-S-H properties, especially for long-term durability, decalcification, etc. [243–245]. Computational models could be a great tool to further investigate differences between suggested C-S-H models and determine their stability [246].

Another interesting point that could be explored with computational models is the stacking faults and orientation of the C-S-H layers and silicate chains. In tobermorite, both the layers and the chains are perfectly aligned. A key aspect for the stability of a disordered material is the maximization of its entropy, or in other words, the number of possible configurations for a given thermodynamic state, and those defects would increase dramatically the entropy of the system and hence its (meta)stability. In fact, it has been already suggested that stacking faults could be necessary to reproduce the C-S-H XRD patterns. Furthermore, atomistic simulation is an appropriate tool to explore the configurational space, looking for new or exotic structures, like C-S-H nanotubes [247], C-S-H nanoparticles, and clusters based on different crystalline phases like xonotlite, etc.

The next frontier in the C-S-H gel atomic structure determination must be linked to investigations of its nucleation and growth mechanism. If we understand how the solid C-S-H "particles" are formed, we would implicitly obtain very detailed information of their structure. From an experimental point of view, recent papers have explored in great detail the structure development during the heterogeneous nucleation of C-S-H and portlandite [248–250]. Atomistic simulations could be used as a complementary technique to understand the process. Despite unraveling nucleation and growth mechanisms of crystals and nanoparticles is a complex problem for atomistic simulations, recent advances in the field are opening new possibilities [251–254].

7. Conclusions

After decades of research, the C-S-H gel continues to be a thorn in the flesh in the field of cement science. Its structure, composition, nucleation and growth, and durability are recurrent research topics, and different models are used to rationalize the results. In this review, we have made a tour of the most relevant empirical and computational C-S-H models proposed over the years.

Taylor's tobermorite-like structure and Richardson's stoichiometry are the accepted empirical C-S-H descriptions by the community. However, many important details remain unsettled, as the presence of

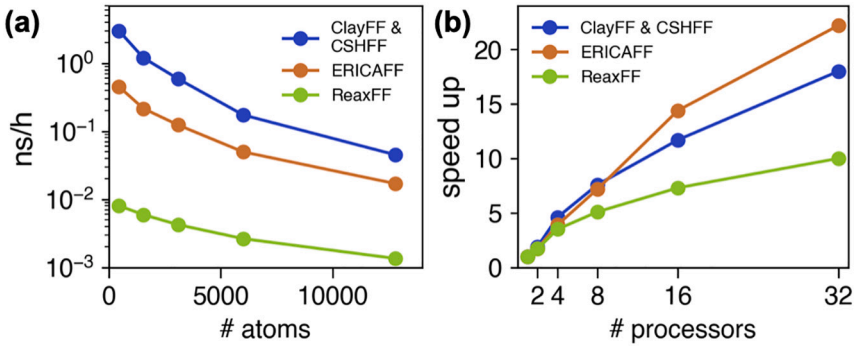

Fig. 11. (a) Simulated time (ns) in 1 h of real time using 8 cores as a function of the system size for different FFs. The ClayFF and CSHFF times overlap and are shown together. (b) Speed up as a function of the number of processors used for the simulation for the selected FFs.

nanoportlandite at high Ca/Si ratios. Computational C-S-H models and atomistic simulations have burst onto in the last years, aiming to bring some light to these uncertainties, and explore nanoscale properties hardly accessible to experiments. We have reviewed the historic development of C-S-H computational models, from the early attempts with simple models to the current realistic disordered tobermorite-like structures. Then, we have inspected the main application of these C-S-H models to investigate Aluminum incorporation to the silicate chains, C-S-H elasticity and mechanics, water and ion mobility within the C-S-H nanopores, and recent studies of C-S-H/organic systems. Finally, we discussed practical aspects of the main computational models, as well as give some hints on possible future directions.

Overall, we hope that this paper will serve as a good reference guide for researchers in the field, giving a global vision of the empirical and computational C-S-H models and their common applications.

CRediT authorship contribution statement

Eduardo Duque-Redondo: Conceptualization, Investigation, Writing – original draft, Writing – review & editing, Supervision. **Patrick A. Bonnaud:** Investigation, Writing – original draft, Writing – review & editing. **Hegoi Manzano:** Conceptualization, Investigation, Writing – original draft, Writing – review & editing, Supervision, Project administration.

Declaration of competing interest

The authors declare that they have no known competing financial interests or personal relationships that could have appeared to influence the work reported in this paper.

Acknowledgments

The authors would like to acknowledge funding from “Departamento de Educación, Política Lingüística y Cultura del Gobierno Vasco” (Grant No. IT912-16 and IT1639-22) and the technical and human support provided by the Scientific Computing Service of SGIker (UPV/EHU/ERDF, EU). E.D.-R. also acknowledges the postdoctoral fellowship from “Programa Posdoctoral de Perfeccionamiento de Personal Investigador Doctor” of the Basque Government.

References

[1] C.F. Ferraris, K.H. Obla, R. Hill, The influence of mineral admixtures on the rheology of cement paste and concrete, Cem. Concr. Res. 31 (2001) 245–255.
[2] D.P. Bentz, A review of early-age properties of cement-based materials, Cem. Concr. Res. 38 (2008) 196–204.
[3] S. Hanehara, K. Yamada, Interaction between cement and chemical admixture from the point of cement hydration, absorption behaviour of admixture, and paste rheology, Cem. Concr. Res. 29 (1999) 1159–1165.
[4] C.L. Page, M.M. Page, Durability of Concrete and Cement Composites, Elsevier, 2007.
[5] G. Land, D. Stephan, The effect of synthesis conditions on the efficiency of csh seeds to accelerate cement hydration, Cem. Concr. Compos. 87 (2018) 73–78.
[6] B. Şimşek, T. Uygunoğlu, Multi-response optimization of polymer blended concrete: a topsis based taguchi application, Constr. Build. Mater. 117 (2016) 251–262.
[7] Y.F. Houst, P. Bowen, F. Perche, A. Kauppi, P. Borget, L. Galmiche, J.-F.Le Meins, F. Lafuma, R.J. Flatt, I. Schober, P.F. Banfill, D.S. Swift, B.O. Myrvold, B. G. Petersen, K. Reknes, Design and function of novel superplasticizers for more durable high performance concrete (superplast project), Cem. Concr. Res. 38 (2008) 1197–1209.
[8] A. Kumar, B.J. Walder, A. Kunhi Mohamed, A. Hofstetter, B. Srinivasan, A. J. Rossini, K. Scrivener, L. Emsley, P. Bowen, The atomic-level structure of cementitious calcium silicate hydrate, J. Phys. Chem. C 121 (2017) 17188–17196.
[9] R. Shahsavari, S.H. Hwang, Size-and shape-controlled synthesis of calcium silicate particles enables self-assembly and enhanced mechanical and durability properties, Langmuir 34 (2018) 12154–12166.
[10] M. Diez-Garcia, J.J. Gaitero, J.S. Dolado, C. Aymonier, Ultra-fast supercritical hydrothermal synthesis of tobermorite under thermodynamically metastable conditions, Angew. Chem. 129 (2017) 3210–3215.
[11] J. Wu, Y.-J. Zhu, F. Chen, Ultrathin calcium silicate hydrate nanosheets with large specific surface areas: synthesis, crystallization, layered self-assembly and applications as excellent adsorbents for drug, protein, and metal ions, Small 9 (2013) 2911–2925.
[12] E. Ogur, R. Botti, M. Bortolotti, P. Colombo, C. Vakifahmetoglu, Synthesis and additive manufacturing of calcium silicate hydrate scaffolds, J. Mater. Res. Technol. 11 (2021) 1142–1151.
[13] P. Yu, R.J. Kirkpatrick, B. Poe, P.F. McMillan, X. Cong, Structure of calcium silicate hydrate (C-S-H): near-, mid-, and far-infrared spectroscopy, J. Am. Ceram. Soc. 82 (1999) 742–748.
[14] A.J. Allen, J.J. Thomas, H.M. Jennings, Composition and density of nanoscale calcium–silicate–hydrate in cement, Nat. Mater. 6 (2007) 311–316.
[15] P.J. Monteiro, G. Geng, D. Marchon, J. Li, P. Alapati, K.E. Kurtis, M.J.A. Qomi, Advances in characterizing and understanding the microstructure of cementitious materials, Cem. Concr. Res. 124 (2019), 105806.
[16] L.B. Skinner, S.R. Chae, C.J. Benmore, H.R. Wenk, P.J.M. Monteiro, Nanostructure of calcium silicate hydrates in cements, Phys. Rev. Lett. 104 (2010) 4.
[17] H.F.W. Taylor, Nanostructure of C-S-H: current status, Adv. Cem. Based Mater. 1 (1993) 38–46.
[18] E. Fratini, F. Ridi, S.-H. Chen, P. Baglioni, Hydration water and microstructure in calcium silicate and aluminate hydrates, J. Phys. Condens. Matter 18 (2006), S2467.
[19] A. Cuesta, J.D. Zea-Garcia, D. Londono-Zuluaga, G. Angeles, I. Santacruz, O. Vallcorba, M. Dapiaggi, S.G. Sanfélix, M.A. Aranda, Multiscale understanding of tricalcium silicate hydration reactions, Sci. Rep. 8 (2018) 1–11.
[20] I.G. Richardson, The calcium silicate hydrates, Cem. Concr. Res. 38 (2008) 137–158.
[21] C. Biagioni, S. Merlino, E. Bonaccorsi, The tobermorite supergroup: a new nomenclature, Mineral. Mag. 79 (2015) 485–495.
[22] S. Grangeon, F. Claret, C. Lerouge, F. Warmont, T. Sato, S. Anraku, C. Numako, Y. Linard, B. Lanson, On the nature of structural disorder in calcium silicate hydrates with a calcium/silicon ratio similar to tobermorite, Cem. Concr. Res. 52 (2013) 31–37.
[23] M.C. Day, F.C. Hawthorne, A structure hierarchy for silicate minerals: chain, ribbon, and tube silicates, Mineral. Mag. 84 (2020) 165–244.
[24] S. Merlino, E. Bonaccorsi, T. Armbruster, The real structures of clinotobermorite and tobermorite 9 Å: OD character, polytypes, and structural relationships, Eur. J. Mineral. 12 (2000) 411–429.
[25] E. Bonaccorsi, S. Merlino, Modular microporous minerals: cancrinite-davyne group and csh phases, Rev. Mineral. Geochem. 57 (2005) 241–290.
[26] R.-M. Pellenq, N. Lequeux, H. Van Damme, Engineering the bonding scheme in c–s–h: the iono-covalent framework, Cem. Concr. Res. 38 (2008) 159–174.
[27] S. Merlino, E. Bonaccorsi, T. Armbruster, The real structure of tobermorite 11A: normal and anomalous forms, OD character and polytypic modifications, Eur. J. Mineral. 13 (2001) 577–590.
[28] R. Dupuis, J. Moon, Y. Jeong, R. Taylor, S.-H. Kang, H. Manzano, A. Ayuela, P. J. Monteiro, J.S. Dolado, Normal and anomalous self-healing mechanism of crystalline calcium silicate hydrates, Cem. Concr. Res. 142 (2021), 106356.
[29] P. Rejmak, J.S. Dolado, M.J. Stott, A. Ayuela, 29Si NMR in cement: a theoretical study on calcium silicate hydrates, J. Phys. Chem. C 116 (2012) 9755–9761.
[30] S. Hamid, The crystal structure of the 11 Å natural tobermorite Ca2. 25 [Si3O7. 5 (OH) 1.5]. 1H2O, Z. Krist. 154 (1981) 189–198.
[31] I.G. Richardson, Tobermorite/jennite- and tobermorite/ calcium hydroxide-based models for the structure of C-S-H: applicability to hardened pastes of tricalcium silicate, -dicalcium silicate, Portland cement, and blends of Portland cement with blast-furnace slag, metakaolin, or silica fume, Cem. Concr. Res. 34 (2004) 1733–1777.
[32] I.L. Moudrakovski, R. Alizadeh, J.J. Beaudoin, Natural abundance high field 43ca solid state nmr in cement science, Phys. Chem. Chem. Phys. 12 (2010) 6961–6969.
[33] P. Rejmak, J.S. Dolado, M.J. Stott, A. Ayuela, 29si nmr in cement: a theoretical study on calcium silicate hydrates, J. Phys. Chem. C 116 (2012) 9755–9761.
[34] S. Grangeon, A. Fernandez-Martinez, A. Baronnet, N. Marty, A. Poulain, E. Elkaïm, C. Roosz, S. Gaboreau, P. Henocq, F. Claret, Quantitative X-ray pair distribution function analysis of nanocrystalline calcium silicate hydrates: a contribution to the understanding of cement chemistry, J. Appl. Crystallogr. 50 (2017) 14–21.
[35] A. Carpenter, R. Chalmers, J. Gard, K. Speakman, H. Taylor, Jennite, a new mineral, Am. Mineral. 51 (1966) 56–74.
[36] N. Hara, N. Inoue, Formation of jennite from fumed silica, Cem. Concr. Res. 10 (1980) 677–682.
[37] J.D. Bernal, The structures of cement hydration compounds, in: Proc. 3rd Int. Symp. Chem. Cem., London volume 1954, 1952, pp. 216–236.
[38] J.D. Bernal, J.W. Jeffery, H.F.W. Taylor, Crystallographic research on the hydration of Portland cement. A first repohttps: on investigations in progress, Mag. Concr. Res. 4 (1952) 49–54.
[39] L.G. Shpynova, N. Id, N.V. Belov, Microstructure of alite cement stone (hydrated tricalcium silicate), in: Soviet Physics Crystallography, USSR 11, 1967, pp. 747–751.
[40] Å. Grudemo, The Crystal Structures of Cement Hydration. A Review and a New Gel Structure Model, Cement och Betong Institutet, 1986.
[41] X.D. Cong, R.J. Kirkpatrick, O-17 MAS NMR investigation of the structure of calcium silicate hydrate gel, J. Am. Ceram. Soc. 79 (1996) 1585–1592.

[42] A.R. Brough, C.M. Dobson, I.G. Richardson, G.W. Groves, In situ solid-state NMR studies of Ca3SiO5: hydration at room temperature and at elevated temperatures using 29Si enrichment, J. Mater. Sci. 29 (1994) 3926–3940.
[43] H.F.W. Taylor, J.W. Howison, Relationships between calcium silicates and clay minerals, Clay Miner. Bull. 3 (1956) 98–111.
[44] H.G. Kurczyk, H.E. Schwiete, Concerning the hydration products of C3S and -C2S, in: Proceedings of the 4th International Symposium on the Chemistry of Cement volume 1, 1962, pp. 349–358.
[45] H.-G. Kurczyk, H.E. Schwiete, Elektronenmikroskopische und thermochemische untersuchungen über die hydratation der calciumsilikate 3 CaO. SiO2 und [beta]-2 CaO. SiO2 und den einfluss von calciumchlorid und gips auf den hydratationsvorgang, Tonind-Ztg Keram. Rundsch. 84 (1960) 585–598.
[46] D.L. Kantro, S. Brunauer, C.H. Weise, Development of surface in the hydration of calcium silicates. II. Extension of investigations to earlier and later stages of hydration, J. Phys. Chem. 66 (1962) 1804–1809.
[47] K. Fujii, W. Kondo, Communications of the American Ceramic Society estimation of thermochemical data for calcium silicate hydrate (C-S-H), J. Am. Ceram. Soc. 66 (1983). C220–C221.
[48] H. Stade, W. Wieker, Zum Aufbau schlecht geordneter Calciumhydrogensilicate. I. Bildung und Eigenschaften einer schlecht geordneten Calciumhydrogendisilicatphase, Z. Anorg. Allg. Chem. 466 (1980) 55–70.
[49] H. Stade, Zum Aufbau Schlecht geordneter Calciumhydrogensilicate. II. Über eine aus Poly-und Disilicat bestehende Phase, Z. Anorg. Allg. Chem. 470 (1980) 69–83.
[50] F.P. Glasser, E.E. Lachowski, D.E. Macphee, Compositional model for calcium silicate hydrate (c-s-h) gels, their solubilities, and free energies of formation, J. Am. Ceram. Soc. 70 (1987) 481–485.
[51] H.F.W. Taylor, Proposed structure for calcium silicate hydrate gel, J. Am. Ceram. Soc. 69 (1986) 464–467.
[52] I.G. Richardson, G.W. Groves, Models for the composition and structure of calcium silicate hydrate (C-S-H) gel in hardened tricalcium silicate pastes, Cem. Concr. Res. 22 (1992) 1001–1010.
[53] I.G. Richardson, Tobermorite/jennite- and tobermorite/calcium hydroxide-based models for the structure of C-S-H: applicability to hardened pastes of tricalcium silicate, beta-dicalcium silicate, Portland cement, and blends of Portland cement with blast-fumace slag, metaka, Cem. Concr. Res. 34 (2004) 1733–1777.
[54] I.G. Richardson, G.W. Groves, The incorporation of minor and trace elements into calcium silicate hydrate (C-S-H) gel in hardened cement pastes, Cem. Concr. Res. 23 (1993) 131–138.
[55] I.G. Richardson, A.R. Brough, R. Brydson, G.W. Groves, C.M. Dobson, Location of aluminum in substituted calcium silicate hydrate (C-S-H) gels as determined by 29Si and 27Al NMR and EELS, J. Am. Ceram. Soc. 76 (1993) 2285–2288.
[56] I.G. Richardson, G.W. Groves, The structure of the calcium silicate hydrate phase present in hardened pastes of white Portland cement/blast-furnace slag blends, J. Mater. Sci. 32 (1997) 4793–4802.
[57] I.G. Richardson, The nature of the hydration products in hardened cement pastes, Cem. Concr. Compos. 22 (2000) 97–113.
[58] I.G. Richardson, J.G. Cabrera, The nature of C-S-H in model slag-cements, Cem. Concr. Compos. 22 (2000) 259–266.
[59] I.G. Richardson, Model structures for C-(A)-S-H(I), Acta Crystallogr. B 70 (2014) 903–923.
[60] X. Cong, R.J. Kirkpatrick, 29Si MAS NMR study of the structure of calcium silicate hydrate, Adv. Cem. Based Mater. 3 (1996) 144–156.
[61] A. Nonat, X. Lecoq, The structure, stoichiometry and properties of csh prepared by c 3 s hydration under controlled condition, in: Nuclear Magnetic Resonance Spectroscopy of Cement-based Materials, Springer, 1998, pp. 197–207.
[62] A. Nonat, The structure and stoichiometry of csh, Cem. Concr. Res. 34 (2004) 1521–1528.
[63] E. Gartner, I. Maruyama, J. Chen, A new model for the csh phase formed during the hydration of Portland cements, Cem. Concr. Res. 97 (2017) 95–106.
[64] J.J. Chen, J.J. Thomas, H.F.W. Taylor, H.M. Jennings, Solubility and structure of calcium silicate hydrate, Cem. Concr. Res. 34 (2004) 1499–1519.
[65] D.A. Kulik, Improving the structural consistency of csh solid solution thermodynamic models, Cem. Concr. Res. 41 (2011) 477–495.
[66] M.W. Grutzeck, A new model for the formation of calcium silicate hydrate (CSH), Mater. Res. Innov. 3 (1999) 160–170.
[67] M.W. Grutzeck, S. Kwan, J.L. Thompson, A. Benesi, A sorosilicate model for calcium silicate hydrate (C–S–H), J. Mater. Sci. Lett. 18 (1999) 217–220.
[68] J.H. Crawford, L.M. Slifkin, Point Defects in Solids: General and Ionic Crystals, Springer Science & Business Media, 2013.
[69] P. Faucon, J. Delaye, J. Virlet, Molecular dynamics simulation of the structure of calcium silicate hydrates: I. ca4+ xsi6o14+ 2x (oh) 4- 2x (h2o) 2 (0 x 1), J. Solid State Chem. 127 (1996) 92–97.
[70] P. Faucon, J.M. Delaye, J. Virlet, J.F. Jacquinot, F. Adenot, Study of the structural properties of the C-S-H (I) by molecular dynamics simulation, Cem. Concr. Res. 27 (1997) 1581–1590.
[71] A.G. Kalinichev, R.J. Kirkpatrick, Molecular dynamics modeling of chloride binding to the surfaces of calcium hydroxide, hydrated calcium aluminate, and calcium silicate phases, Chem. Mater. 14 (2002) 3539–3549.
[72] R.T. Cygan, J.-J. Liang, A.G. Kalinichev, Molecular models of hydroxide, oxyhydroxide, and clay phases and the development of a general force field, J. Phys. Chem. B 108 (2004) 1255–1266.
[73] A.G. Kalinichev, J.W. Wang, R.J. Kirkpatrick, Molecular dynamics modeling of the structure, dynamics and energetics of mineral-water interfaces: application to cement materials, Cem. Concr. Res. 37 (2007) 337–347.
[74] A. Gmira, M. Zabat, R.J.M. Pellenq, H. Van Damme, Microscopic physical basis of the poromechanical behavior of cement-based materials, Mater. Struct. 37 (2004) 3–14.
[75] H. Manzano, J.S. Dolado, A. Guerrero, A. Ayuela, Mechanical properties of crystalline calcium-silicate-hydrates: comparison with cementitious C-S-H gels, Phys. Status Solidi (a) 204 (2007) 1775–1780.
[76] H. Manzano, J.S. Dolado, A. Ayuela, Elastic properties of the main species present in Portland cement pastes, Acta Mater. 57 (2009) 1666–1674.
[77] J.S. Dolado, M. Griebel, J. Hamaekers, A molecular dynamic study of cementitious calcium silicate hydrate (C–S–H) gels, J. Am. Ceram. Soc. 90 (2007) 3938–3942.
[78] D.A. Litton, S.H. Garofalini, Modeling of hydrophilic wafer bonding by molecular dynamics simulations, J. Appl. Phys. 89 (2001) 6013–6023.
[79] E. Bonaccorsi, S. Merlino, A.R. Kampf, The crystal structure of tobermorite 14 å (plombierite), a c–s–h phase, J. Am. Ceram. Soc. 88 (2005) 505–512.
[80] E. Bonaccorsi, S. Merlino, H. Taylor, The crystal structure of jennite, ca9si6o18 (oh) 6. 8h2o, Cem. Concr. Res. 34 (2004) 1481–1488.
[81] R.J.M. Pellenq, A. Kushima, R. Shahsavari, K.J. Van Vliet, M.J. Buehler, S. Yip, F. J. Ulm, A realistic molecular model of cement hydrates, Proc. Natl. Acad. Sci. U. S. A. 106 (2009) 16102–16107.
[82] A. Ayuela, J.S. Dolado, I. Campillo, Y.R. De Miguel, E. Erkizia, D. Sánchez-Portal, A. Rubio, A. Porro, P.M. Echenique, Silicate chain formation in the nanostructure of cement-based materials, J. Chem. Phys. 127 (2007), 164710.
[83] N. Lequeux, A. Morau, S. Philippot, P. Boch, Extended x-ray absorption fine structure investigation of calcium silicate hydrates, J. Am. Ceram. Soc. 82 (1999) 1299–1306.
[84] Y. Janik, W. Kurdowski, R. Podsiadly, J. Samseth, Fractal structure of csh and tobermorite phases, Acta Phys. Pol. A 100 (2001) 529–538.
[85] G. Constantinides, F.J. Ulm, The effect of two types of C-S-H on the elasticity of cement-based materials: results from nanoindentation and micromechanical modeling, Cem. Concr. Res. 34 (2004) 67–80.
[86] G. Constantinides, F.J. Ulm, The nanogranular nature of C-S-H, J. Mech. Phys. Solids 55 (2007) 64–90.
[87] M.J. Abdolhosseini Qomi, K.J. Krakowiak, M. Bauchy, K.L. Stewart, R. Shahsavari, D. Jagannathan, D.B. Brommer, A. Baronnet, M.J. Buehler, S. Yip, F.-J. Ulm, K.J. Van Vliet, R.J.M. Pellenq, M.J.A. Qomi, K.J. Krakowiak, M. Bauchy, K.L. Stewart, R. Shahsavari, D. Jagannathan, D.B. Brommer, A. Baronnet, M.J. Buehler, S. Yip, Combinatorial molecular optimization of cement hydrates, Nat. Commun. 5 (2014) 1–10.
[88] J.J. Thomas, H.M. Jennings, A.J. Allen, Relationships between composition and density of tobermorite, jennite, and nanoscale CaO- SiO2- H2O, J. Phys. Chem. C 114 (2010) 7594–7601.
[89] I.G. Richardson, The importance of proper crystal-chemical and geometrical reasoning demonstrated using layered single and double hydroxides, Acta Crystallogr. Sect. B: Struct. Sci. Cryst. Eng. Mater. 69 (2013) 150–162.
[90] S. Garrault, E. Finot, E. Lesniewska, A. Nonat, Study of CSH growth on C 3 S surface during its early hydration, Mater. Struct. 38 (2005) 435–442.
[91] H. Manzano, S. Moeini, F. Marinelli, A.C.T. van Duin, F.-J. Ulm, R.J.M. Pellenq, Confined water dissociation in microporous defective silicates: mechanism, dipole distribution, and impact on substrate properties, J. Am. Chem. Soc. 134 (2012) 2208–2215.
[92] J.C. Fogarty, H.M. Aktulga, A.Y. Grama, A.C.T. van Duin, S.A. Pandit, A reactive molecular dynamics simulation of the silica-water interface, J. Chem. Phys. 132 (2010), 174704_1–174704_10.
[93] H. Manzano, R.J. Pellenq, F.-J. Ulm, M.J. Buehler, A.C. van Duin, Hydration of calcium oxide surface predicted by reactive force field molecular dynamics, Langmuir 28 (2012) 4187–4197.
[94] R. Shahsavari, R.J.-M. Pellenq, F.-J. Ulm, Empirical force fields for complex hydrated calcio-silicate layered materials, Phys. Chem. Chem. Phys. 13 (2011) 1002–1011.
[95] G. Kovačević, B. Persson, L. Nicoleau, A. Nonat, V. Veryazov, Atomistic modeling of crystal structure of Ca1.67SiHx, Cem. Concr. Res. 67 (2015) 197–203.
[96] Y. Chiang, S.-W. Chang, Bridging the gap between nmr measured mean silicate chain length and nano-scale silicate polymorphism of calcium silicate hydrates, Cem. Concr. Res. 140 (2021), 106268.
[97] A.K. Mohamed, S.C. Parker, P. Bowen, S. Galmarini, An atomistic building block description of csh-towards a realistic csh model, Cem. Concr. Res. 107 (2018) 221–235.
[98] A. Kunhi Mohamed, P. Moutzouri, P. Berruyer, B.J. Walder, J. Siramanont, M. Harris, M. Negroni, S.C. Galmarini, S.C. Parker, K.L. Scrivener, L. Emsley, P. Bowen, The atomic-level structure of cementitious calcium aluminate silicate hydrate, J. Am. Chem. Soc. 142 (2020) 11060–11071. PMID: 32406680.
[99] F. Basquiroto de Souza, K. Sagoe-Crentsil, W. Duan, Determining the disordered nanostructure of calcium silicate hydrate (c-s-h) from broad x-ray diffractograms, J. Am. Ceram. Soc. 105 (2) (2021) 1491–1502.
[100] P. Tasker, The stability of ionic crystal surfaces, J. Phys. C Solid State Phys. 12 (1979) 4977.
[101] E. Duque-Redondo, H. Manzano, N. Epelde-Elezcano, V. Martínez-Martínez, I. López-Arbeloa, Molecular forces governing shear and tensile failure in clay-dye hybrid materials, Chem. Mater. 26 (2014) 4338–4345.
[102] E. Duque-Redondo, I. López-Arbeloa, H. Manzano, Distinctive diffusion regimes of organic molecules in clays:(de) coupled motion with water, J. Phys. Chem. C 123 (2018) 511–516.
[103] H. Heinz, H. Ramezani-Dakhel, Simulations of inorganic–bioorganic interfaces to discover new materials: insights, comparisons to experiment, challenges, and opportunities, Chem. Soc. Rev. 45 (2016) 412–448.

[104] B. Chen, J.R. Evans, H.C. Greenwell, P. Boulet, P.V. Coveney, A.A. Bowden, A. Whiting, A critical appraisal of polymer–clay nanocomposites, Chem. Soc. Rev. 37 (2008) 568–594.
[105] N. Loganathan, A.O. Yazaydin, G.M. Bowers, A.G. Kalinichev, R.J. Kirkpatrick, Molecular dynamics study of co2 and h2o intercalation in smectite clays: effect of temperature and pressure on interlayer structure and dynamics in hectorite, J. Phys. Chem. C 121 (2017) 24527–24540.
[106] R.T. Cygan, J.A. Greathouse, A.G. Kalinichev, Advances in clayff molecular simulation of layered and nanoporous materials and their aqueous interfaces, J. Phys. Chem. C 125 (2021) 17573–17589.
[107] T. Jamil, A. Javadi, H. Heinz, Mechanism of molecular interaction of acrylate-polyethylene glycol acrylate copolymers with calcium silicate hydrate surfaces, Green Chem. 22 (2020) 1577–1593.
[108] M.D. Andersen, H.J. Jakobsen, J. Skibsted, Incorporation of aluminum in the calcium silicate hydrate (c- s- h) of hydrated Portland cements: a high-field 27al and 29si mas nmr investigation, Inorg. Chem. 42 (2003) 2280–2287.
[109] M.D. Andersen, H.J. Jakobsen, J. Skibsted, A new aluminium-hydrate species in hydrated Portland cements characterized by 27al and 29si mas nmr spectroscopy, Cem. Concr. Res. 36 (2006) 3–17.
[110] G. Sun, J.F. Young, R.J. Kirkpatrick, The role of al in c–s–h: nmr, xrd, and compositional results for precipitated samples, Cem. Concr. Res. 36 (2006) 18–29.
[111] I.G. Richardson, A.R. Brough, R. Brydson, G.W. Groves, C.M. Dobson, Location of aluminum in substituted calcium silicate hydrate (c-s-h) gels as determined by 29si and 27al nmr and eels, J. Am. Ceram. Soc. 76 (1993) 2285–2288.
[112] X. Pardal, F. Brunet, T. Charpentier, I. Pochard, A. Nonat, 27al and 29si solid-state nmr characterization of calcium-aluminosilicate-hydrate, Inorg. Chem. 51 (2012) 1827–1836.
[113] P. Faucon, A. Delagrave, J. Petit, C. Richet, J. Marchand, H. Zanni, Aluminum incorporation in calcium silicate hydrates (c- s- h) depending on their ca/si ratio, J. Phys. Chem. B 103 (1999) 7796–7802.
[114] S. Kashihara, S. Yamanaka, T. Inoue, T. Komatsu, H. Toyoshima, Quantum chemical determination of the al-substituted site in tobermorite, J. Am. Ceram. Soc. 77 (1994) 3023–3026.
[115] H. Manzano, J.S. Dolado, A. Ayuela, Aluminum incorporation to dreierketten silicate chains, J. Phys. Chem. B 113 (2009) 2832–2839.
[116] L. Pegado, C. Labbez, S.V. Churakov, Mechanism of aluminium incorporation into c–s–h from ab initio calculations, J. Mater. Chem. A 2 (2014) 3477–3483.
[117] M.J. Abdolhosseini Qomi, F.-J. Ulm, R.J.-M. Pellenq, Evidence on the dual nature of aluminum in the calcium-silicate-hydrates based on atomistic simulations, J. Am. Ceram. Soc. 95 (2012) 1128–1137.
[118] H. Manzano, J.S. Dolado, M. Griebel, J. Hamaekers, A molecular dynamics study of the aluminosilicate chains structure in Al-rich calcium silicate hydrated (C-S-H) gels, Phys. Status Solidi (a) 205 (2008) 1324–1329.
[119] H. Manzano, E. Durgun, M.J. Abdolhosseine Qomi, F.-J. Ulm, R.J. Pellenq, J. C. Grossman, Impact of chemical impurities on the crystalline cement clinker phases determined by atomistic simulations, Cryst. Growth Des. 11 (2011) 2964–2972.
[120] D. Fan, S. Yang, Mechanical properties of csh globules and interfaces by molecular dynamics simulation, Constr. Build. Mater. 176 (2018) 573–582.
[121] W. Lin, C. Zhang, J. Fu, H. Xin, Dynamic mechanical behaviors of calcium silicate hydrate under shock compression loading using molecular dynamics simulation, J. Non-Cryst. Solids 500 (2018) 482–486.
[122] Y. Zhang, Q. Zhou, J.W. Ju, M. Bauchy, New insights into the mechanism governing the elasticity of calcium silicate hydrate gels exposed to high temperature: a molecular dynamics study, Cem. Concr. Res. 141 (2021), 106333.
[123] J. Fu, F. Bernard, S. Kamali-Bernard, Assessment of the elastic properties of amorphous calcium silicates hydrates (i) and (ii) structures by molecular dynamics simulation, Mol. Simul. 44 (2018) 285–299.
[124] Y. Liang, Mechanical and fracture properties of calcium silicate hydrate and calcium hydroxide composite from reactive molecular dynamics simulations, Chem. Phys. Lett. 761 (2020), 138117.
[125] J. Zhou, Y. Liang, Effect of water on the dynamic tensile mechanical properties of calcium silicate hydrate: based on molecular dynamics simulation, Materials 12 (2019) 2837.
[126] Q. Zheng, J. Jiang, J. Yu, X. Li, S. Li, Aluminum-induced interfacial strengthening in calcium silicate hydrates: structure, bonding, and mechanical properties, ACS Sustain. Chem. Eng. 8 (2020) 2622–2631.
[127] R. Shahsavari, M.J. Buehler, R.J.M. Pellenq, F.J. Ulm, First-principles study of elastic constants and interlayer interactions of complex hydrated oxides: case of study of tobermorite and jennite, J. Am. Ceram. Soc. 92 (2009) 2323–2330.
[128] H. Manzano, E. Masoero, I. Lopez-Arbeloa, H.M. Jennings, Shear deformations in calcium silicate hydrates, Soft Matter 9 (2013) 7333–7341.
[129] J.E. Oh, S.M. Clark, H.R. Wenk, P.J. Monteiro, Experimental determination of bulk modulus of 14 åtobermorite using high pressure synchrotron x-ray diffraction, Cem. Concr. Res. 42 (2012) 397–403.
[130] J.K. Su, S.W. Cho, C.C. Yang, R. Huang, Effect of sand ratio on the elastic modulus of self-compacting concrete, J. Mar. Sci. Technol. 10 (2002) 8–13.
[131] G. Geng, R.J. Myers, M.J.A. Qomi, P.J.M. Monteiro, Densification of the interlayer spacing governs the nanomechanical properties of calcium-silicate-hydrate, Sci. Rep. 7 (2017) 10986.
[132] P.A. Bonnaud, Q. Ji, K.J. Van Vliet, Effects of elevated temperature on the structure and properties of calcium-silicate-hydrate gels: the role of confined water, Soft Matter 9 (2013) 6418–6429.
[133] D. Hou, J. Yu, A. Hanif, Molecular dynamics study on calcium silicate hydrate subjected to tension loading and water attack: structural evolution, dynamics degradation and reactivity mechanism, Phys. Chem. Chem. Phys. 20 (2018) 11130–11144.
[134] I. Maruyama, T. Ohkubo, T. Haji, R. Kurihara, Dynamic microstructural evolution of hardened cement paste during first drying monitored by 1h nmr relaxometry, Cem. Concr. Res. 122 (2019) 107–117.
[135] P. Suwanmaneechot, A. Aili, I. Maruyama, Creep behavior of csh under different drying relative humidities: interpretation of microindentation tests and sorption measurements by multi-scale analysis, Cem. Concr. Res. 132 (2020), 106036.
[136] J. Li, W. Zhang, P.J. Monteiro, Preferred orientation of calcium aluminosilicate hydrate compacts: implications for creep and indentation, Cem. Concr. Res. 143 (2021), 106371.
[137] S.D. Palkovic, S. Moeini, S. Yip, O. Büyüköztürk, Mechanical behavior of a composite interface: calcium-silicate-hydrates, J. Appl. Phys. 118 (2015), 034305.
[138] A. Morshedifard, S. Masoumi, M.J.Abdolhosseini Qomi, Nanoscale origins of creep in calcium silicate hydrates, Nat. Commun. 9 (2018) 1785.
[139] M. Bauchy, H. Laubie, M.J. Abdolhosseini Qomi, C.G. Hoover, F.-J. Ulm, R.J.-M. Pellenq, Fracture toughness of calcium-silicate-hydrate grains from molecular dynamics simulations, J. Non-Cryst. Solids 419 (2015) 58–64.
[140] G. Constantinides, F.-J. Ulm, The nanogranular nature of c–s–h, J. Mech. Phys. Solids 55 (2007) 64–90.
[141] M. Vandamme, F.-J. Ulm, Nanogranular origin of concrete creep, Proc. Natl. Acad. Sci. 106 (2009) 10552–10557.
[142] P.A. Bonnaud, Q. Ji, B. Coasne, R.J.M. Pellenq, K.J. Van Vliet, Thermodynamics of water confined in porous calcium-silicate-hydrates, Langmuir 28 (2012) 11422–11432.
[143] F.-J. Ulm, O. Coussy, Z.P. Bažant, The "Chunnel" fire I: chemoplastic softening in rapidly heated concrete, J. Eng. Mech. 125 (1999) 272–281.
[144] M.J. DeJong, F.J. Ulm, The nanogranular behavior of C-S-H at elevated temperatures (up to 700 degrees C), Cem. Concr. Res. 37 (2007) 1–12.
[145] P.A. Bonnaud, C. Labbez, R. Miura, A. Suzuki, N. Miyamoto, N. Hatakeyama, A. Miyamoto, K.J. Van Vliet, Interaction grand potential between calcium–silicate–hydrate nanoparticles at the molecular level, Nanoscale 8 (2016) 4160–4172.
[146] C. Plassard, E. Lesniewska, I. Pochard, A. Nonat, Nanoscale experimental investigation of particle interactions at the origin of the cohesion of cement, Langmuir 21 (2005) 7263–7270.
[147] S. Masoumi, H. Valipour, M.J.A. Qomi, Intermolecular forces between nanolayers of crystalline calcium-silicate-hydrates in aqueous medium, J. Phys. Chem. C 121 (2017), 164714.
[148] S. Masoumi, S. Zare, H. Valipour, M.J.A. Qomi, Effective interactions between calcium-silicate-hydrate nanolayers, J. Phys. Chem. C 123 (2019) 4755–4766.
[149] T. Pan, K. Xia, L. Wang, Chloride binding to calcium silicate hydrates (C-S-H) in cement paste: a molecular dynamics analysis, Int. J. Pavement Eng. 11 (2010) 2010.
[150] J. Jiang, P. Wang, D. Hou, The mechanism of cesium ions immobilization in the nanometer channel of calcium silicate hydrate: a molecular dynamics study, Phys. Chem. Chem. Phys. 19 (2017) 27974–27986.
[151] Y. Zhou, D. Hou, J. Jiang, P. Wang, Chloride ions transport and adsorption in the nano-pores of silicate calcium hydrate: experimental and molecular dynamics studies, Constr. Build. Mater. 4 (2016) 991–1001.
[152] B. Zehtab, A. Tarighat, Diffusion study for chloride ions and water molecules in C-S-H gel in nano-scale using molecular dynamics: case study of tobermorite, Adv. Concr. Constr. 4 (2016) 305–317.
[153] D. Hou, Z. Li, Molecular dynamics study of water and ions transport in nano-pore of layered structure: a case study of tobermorite, Microporous Mesoporous Mater. 195 (2014) 9–20.
[154] P. Wang, Q. Zhang, M. Wang, B. Yin, D. Hou, Y. Zhangab, Atomistic insights into cesium chloride solution transport through the ultra-confined calcium-silicate-Hydrate Channel, Phys. Chem. Chem. Phys. 21 (2019) 11892–11902.
[155] D. Hou, Y. Jia, J. Yu, P. Wang, Q. Liu, Transport properties of sulfate and chloride ions confined between calcium silicate hydrate surfaces: a molecular dynamics study, J. Phys. Chem. C 49 (2018) 28021–28032.
[156] E. Duque-Redondo, K. Yamada, J.S. Dolado, H. Manzano, Microscopic mechanism of radionuclide cs retention in al containing csh nanopores, Comput. Mater. Sci. 190 (2021), 110312.
[157] E. Duque-Redondo, Y. Kazuo, I. López-Arbeloa, H. Manzano, Cs-137 immobilization in csh gel nanopores, Phys. Chem. Chem. Phys. 20 (2018) 9289–9297.
[158] E. Duque-Redondo, K. Yamada, H. Manzano, Cs retention and diffusion in csh at different ca/si ratio, Cem. Concr. Res. 140 (2021), 106294.
[159] P.A.P. Bonnaud, H. Manzano, R. Miura, A. Suzuki, N. Miyamoto, N. Hatakeyama, A. Miyamoto, Temperature dependence of nanoconfined water properties: application to cementitious materials, J. Phys. Chem. C 120 (2016) 11465–11480.
[160] D. Hou, Z. Li, T. Zhao, P. Zhang, Water transport in the nano-pore of the calcium silicate phase: reactivity, structure and dynamics, Phys. Chem. Chem. Phys. 17 (2015) 1411–1423.
[161] D. Li, W. Zhao, D. Hou, T. Zhao, Molecular dynamics study on the chemical bound, physical adsorbed and ultra-confined water molecules in the nano-pore of calcium silicate hydrate, Constr. Build. Mater. 151 (2017) 563–574.
[162] D. Hou, C. Hu, Z. Li, Molecular simulation of the ions ultraconfined in the nanometer-channel of calcium silicate hydrate: hydration mechanism, dynamic properties, and influence on the cohesive strength, Inorg. Chem. 56 (2017) 1881–1896.

[163] Z. Liu, D. Xu, S. Gao, Y. Zhang, J. Jiang, Assessing the adsorption and diffusion behavior of multicomponent ions in saturated calcium silicate hydrate gel pores using molecular dynamics, ACS Sustain. Chem. Eng. 8 (2020) 3718–3727.
[165] Q. Ji, R.J.M. Pellenq, K.J. Van Vliet, Comparison of computational water models for simulation of calcium–silicate–hydrate, Comput. Mater. Sci. 53 (2012) 234–240.
[166] M.J. Abdolhosseini Qomi, M. Bauchy, F.-J. Ulm, R.J.-M. Pellenq, Anomalous composition-dependent dynamics of nano confined water in the interlayer of disordered calcium-silicates, J. Chem. Phys. 140 (5) (2014), 054515.
[169] S. Cerveny, S. Arrest-Igor, J.S. Dolado, J.J. Gaitero, A. Alegrìa, J. Colmenero, Effect of hydration on the dielectric properties of C-S-H gel, J. Chem. Phys. 134 (2011), 034509.
[170] M. Monasterio, H. Jansson, J.J. Gaitero, J.S. Dolado, S. Cerveny, Cause of the fragile-to-strong transition observed in water confined in CSH gel, J. Chem. Phys. 139 (2013), 164714.
[171] T. Honorio, K. Abahri, Non equilibrium molecular dynamics simulation of the hydrodynamics in crystalline calcium silicate hydrates nanopores, in: RILEM Spring Convention and Conference on Sustainable Materials, Systems and Structures (SMSS 2019), RILEM Publications S.A.R.L, 2019, pp. 72–77.
[172] E. Duque-Redondo, K. Yamada, H. Manzano, Effect of chloride and sulfate in the immobilization of cs-137 in csh gel, J. Adv. Concr. Technol. 19 (2021) 95–105.
[173] P. Yu, R.J. Kirkpatrick, 35cl nmr relaxation study of cement hydrate suspensions, Cem. Concr. Res. 31 (2001) 1479–1485.
[174] R. Kirkpatrick, A. Kalinichev, P. Yu, Chloride binding to cement phases: exchange isotherm, exp 35 cl nmr and molecular dynamics modeling studies, Mater. Sci. Concr. Spec. (2001) 77–92.
[175] M. Gou, X. Guan, Q. Sun, Adsorption of chloride ion by calcium silicate hydrate, J. Build. Mater. 18 (2015) 363–368.
[176] Y. Zhou, D. Hou, J. Jiang, L. Liu, W. She, J. Yu, Experimental and molecular dynamics studies on the transport and adsorption of chloride ions in the nano-pores of calcium silicate phase: the influence of calcium to silicate ratios, Microporous Mesoporous Mater. 255 (2018) 23–35.
[177] P. Pivonka, C. Hellmich, D. Smith, Microscopic effects on chloride diffusivity of cement pastes—a scale-transition analysis, Cem. Concr. Res. 34 (2004) 2251–2260.
[178] E. Duque-Redondo, Atomistic Simulations of Confined Species in 2D Nanostructures: Clays and C-S-H Gel, University of the Basque Country, 2018. Ph. D. thesis.
[179] T. Ayub, S.U. Khan, F.A. Memon, Mechanical characteristics of hardened concrete with different mineral admixtures: a review, Sci. World J. 2014 (2014).
[180] V.S. Ramachandran, Concrete Admixtures Handbook: Properties, Science and Technology, William Andrew, 1996.
[181] M. Al-Zahrani, M. Maslehuddin, S. Al-Dulaijan, M. Ibrahim, Mechanical properties and durability characteristics of polymer-and cement-based repair materials, Cem. Concr. Compos. 25 (2003) 527–537.
[182] Y. Ohama, V. Ramachandran, Polymer-modified mortars and concretes, in: Concrete Admixtures Handbook, Elsevier, 1996, pp. 558–656.
[183] V. Riley, I. Razl, Polymer additives for cement composites: a review, Composites 5 (1974) 27–33.
[184] T.M. Aminabhavi, P.E. Cassidy, L.E. Kukacka, Use of polymers in concrete technology, J. Macromol. Sci. C Polym. Rev. J. 22 (1982) 1–55.
[185] B.H. Cho, W. Chung, B.H. Nam, Molecular dynamics simulation of calcium-silicate-hydrate for nano-engineered cement composites—a review, Nanomaterials 10 (2020) 2158.
[186] J. Ha, S. Chae, K. Chou, T. Tyliszczak, P. Monteiro, Effect of polymers on the nanostructure and on the carbonation of calcium silicate hydrates: a scanning transmission x-ray microscopy study, J. Mater. Sci. 47 (2012) 976–989.
[187] J.J. Beaudoin, H. Dramé, L. Raki, R. Alizadeh, Formation and properties of csh–peg nano-structures, Mater. Struct. 42 (2009) 1003–1014.
[188] H. Matsuyama, J.F. Young, Intercalation of polymers in calcium silicate hydrate: a new synthetic approach to biocomposites? Chem. Mater. 11 (1999) 16–19.
[189] R. Khoshnazar, J.J. Beaudoin, L. Raki, R. Alizadeh, Volume stability of calcium-silicate-hydrate/polyaniline nanocomposites in aqueous salt solutions, ACI Mater. J. (2014) 111.
[190] R. Khoshnazar, J.J. Beaudoin, L. Raki, R. Alizadeh, Characteristics and engineering performance of csh/aminobenzoic acid composite systems, J. Adv. Concr. Technol. 13 (2015) 415–420.
[191] F. Pelisser, P. Gleize, A. Mikowski, Structure and micro-nanomechanical characterization of synthetic calcium–silicate–hydrate with poly (vinyl alcohol), Cem. Concr. Compos. 48 (2014) 1–8.
[192] S. Zhang, E. Duque-Redondo, A. Kostiuchenko, J.S. Dolado, G. Ye, Molecular dynamics and experimental study on the adhesion mechanism of polyvinyl alcohol (pva) fiber in alkali-activated slag/fly ash, Cem. Concr. Res. 145 (2021), 106452.
[193] F. Sanchez, L. Zhang, Molecular dynamics modeling of the interface between surface functionalized graphitic structures and calcium–silicate–hydrate: interaction energies, structure, and dynamics, J. Colloid Interface Sci. 323 (2008) 349–358.
[194] M. Krishnan, M. Saharay, R.J. Kirkpatrick, Molecular dynamics modeling of co2 and poly (ethylene glycol) in montmorillonite: the structure of clay–polymer composites and the incorporation of co2, J. Phys. Chem. C 117 (2013) 20592–20609.
[195] A. Lushnikova, A. Zaoui, Improving mechanical properties of csh from inserted carbon nanotubes, J. Phys. Chem. Solids 105 (2017) 72–80.
[196] B. Al-Muhit, F. Sanchez, Nano-engineering of the mechanical properties of tobermorite 14 å with graphene via molecular dynamics simulations, Constr. Build. Mater. 233 (2020), 117237.
[197] M. Pšenička, J. Škoda, M. Pospíšil, Structural arrangement and properties of layered double hydroxide drug nanocarrier intercalated by sulindac and mefenamic acid solved by molecular simulation methods, Appl. Clay Sci. 189 (2020), 105560.
[198] S. Merlino, E. Bonaccorsi, T. Armbruster, Tobermorites: their real structure and order-disorder (od) character, Am. Mineral. 84 (1999) 1613–1621.
[199] H. Alkhateb, A. Al-Ostaz, A.H.-D. Cheng, X. Li, Materials genome for graphene-cement nanocomposites, J. Nanomech. Micromech. 3 (2013) 67–77.
[200] H. Wan, Y. Zhang, Interfacial bonding between graphene oxide and calcium silicate hydrate gel of ultra-high performance concrete, Mater. Struct. 53 (2020) 1–12.
[201] M. Kai, L. Zhang, K. Liew, Graphene and graphene oxide in calcium silicate hydrates: chemical reactions, mechanical behavior and interfacial sliding, Carbon 146 (2019) 181–193.
[202] M. Eftekhari, S. Mohammadi, Molecular dynamics simulation of the nonlinear behavior of the cnt-reinforced calcium silicate hydrate (c–s–h) composite, Compos. A: Appl. Sci. Manuf. 82 (2016) 78–87.
[203] B. Sindu, S. Sasmal, Molecular dynamics simulations for evaluation of surfactant compatibility and mechanical characteristics of carbon nanotubes incorporated cementitious composite, Constr. Build. Mater. 253 (2020), 119190.
[204] Y. Zhou, D. Hou, H. Manzano, C.A. Orozco, G. Geng, P.J. Monteiro, J. Liu, Interfacial connection mechanisms in calcium–silicate–hydrates/polymer nanocomposites: a molecular dynamics study, ACS Appl. Mater. Interfaces 9 (2017) 41014–41025.
[205] D. Hou, J. Yu, P. Wang, Molecular dynamics modeling of the structure, dynamics, energetics and mechanical properties of cement-polymer nanocomposite, Compos. Part B 162 (2019) 433–444.
[206] Y. Zhou, D. Hou, G. Geng, P. Feng, J. Yu, J. Jiang, Insights into the interfacial strengthening mechanisms of calcium-silicate-hydrate/polymer nanocomposites, Phys. Chem. Chem. Phys. 20 (2018) 8247–8266.
[207] D. Hou, J. Yu, P. Wang, Molecular dynamics modeling of the structure, dynamics, energetics and mechanical properties of cement-polymer nanocomposite, Compos. Part B 162 (2019) 433–444.
[208] P. Dauber-Osguthorpe, V.A. Roberts, D.J. Osguthorpe, J. Wolff, M. Genest, A. T. Hagler, Structure and energetics of ligand binding to proteins: Escherichia coli dihydrofolate reductase-trimethoprim, a drug-receptor system, Proteins: Struct., Funct., Bioinf. 4 (1988) 31–47.
[209] Y. Zhou, C.A. Orozco, E. Duque-Redondo, H. Manzano, G. Geng, P. Feng, P. J. Monteiro, C. Miao, Modification of poly (ethylene glycol) on the microstructure and mechanical properties of calcium silicate hydrates, Cem. Concr. Res. 115 (2019) 20–30.
[210] F. Shalchy, N. Rahbar, Nanostructural characteristics and interfacial properties of polymer fibers in cement matrix, ACS Appl. Mater. Interfaces 7 (2015) 17278–17286.
[211] Y. Zhou, J. Cai, D. Hou, H. Chang, J. Yu, The inhibiting effect and mechanisms of smart polymers on the transport of fluids throughout nano-channels, Appl. Surf. Sci. 500 (2020), 144019.
[212] A. Picker, L. Nicoleau, A. Nonat, C. Labbez, H. Cölfen, Identification of binding peptides on calcium silicate hydrate: a novel view on cement additives, Adv. Mater. 26 (2014) 1135–1140.
[213] Q. Han, Y. Yang, J. Zhang, J. Yu, D. Hou, B. Dong, H. Ma, Insights into the interfacial strengthening mechanism of waste rubber/cement paste using polyvinyl alcohol: experimental and molecular dynamics study, Cem. Concr. Compos. 114 (2020), 103791.
[214] E. Hosseini, M. Zakertabrizi, A.H. Korayem, G. Xu, A novel method to enhance the interlayer bonding of 3d printing concrete: an experimental and computational investigation, Cem. Concr. Compos. 99 (2019) 112–119.
[215] I. Androniuk, C. Landesman, P. Henocq, A.G. Kalinichev, Adsorption of gluconate and uranyl on csh phases: combination of wet chemistry experiments and molecular dynamics simulations for the binary systems, Phys. Chem. Earth A/B/C 99 (2017) 194–203.
[216] I. Androniuk, A.G. Kalinichev, Molecular dynamics simulation of the interaction of uranium (vi) with the c–s–h phase of cement in the presence of gluconate, Appl. Geochem. 113 (2020), 104496.
[217] M. Spellings, S.C. Glotzer, Machine learning for crystal identification and discovery, AICHE J. 64 (2018) 2198–2206.
[218] S. Zeng, G. Li, Y. Zhao, R. Wang, J. Ni, Machine learning-aided design of materials with target elastic properties, J. Phys. Chem. C 123 (2019) 5042–5047.
[219] C. Chen, W. Ye, Y. Zuo, C. Zheng, S.P. Ong, Graph networks as a universal machine learning framework for molecules and crystals, Chem. Mater. 31 (2019) 3564–3572.
[220] D.C. Palmer, Visualization and analysis of crystal structures using crystalmaker software, Z. Krist. 230 (2015) 559–572.
[221] K. Momma, F. Izumi, VESTA3 for three-dimensional visualization of crystal, volumetric and morphology data, J. Appl. Crystallogr. 44 (2011) 1272–1276.
[222] M.D. Hanwell, D.E. Curtis, D.C. Lonie, T. Vandermeersch, E. Zurek, G. R. Hutchison, Avogadro: an advanced semantic chemical editor, visualization, and analysis platform, J. Cheminformatics 4 (2012) 1–17.
[223] J.J. Thomas, J.J. Chen, H.M. Jennings, D.A. Neumann, Ca- oh bonding in the c- s-h gel phase of tricalcium silicate and white Portland cement pastes measured by inelastic neutron scattering, Chem. Mater. 15 (2003) 3813–3817.

[224] L. Martínez, R. Andrade, E.G. Birgin, J.M. Martínez, Packmol: a package for building initial configurations for molecular dynamics simulations, J. Comput. Chem. 30 (2009) 2157–2164.
[225] V.O. Özçelik, N. Garg, C.E. White, Symmetry-induced stability in alkali-doped calcium silicate hydrate, J. Phys. Chem. C 123 (2019) 14081–14088.
[226] R. Maddalena, K. Li, P.A. Chater, S. Michalik, A. Hamilton, Direct synthesis of a solid calcium-silicate-hydrate (csh), Constr. Build. Mater. 223 (2019) 554–565.
[227] Y. Yan, S.-Y. Yang, G.D. Miron, I.E. Collings, E. L'Hôpital, J. Skibsted, F. Winnefeld, K. Scrivener, B. Lothenbach, Effect of alkali hydroxide on calcium silicate hydrate (csh), Cem. Concr. Res. 151 (2022), 106636.
[228] A.C. Muller, K.L. Scrivener, A.M. Gajewicz, P.J. McDonald, Densification of c–s–h measured by 1h nmr relaxometry, J. Phys. Chem. C 117 (2013) 403–412.
[229] H. Manzano, A.K. Mohamed, R.K. Mishra, P. Bowen, A discussion on the paper "role of porosity on the stiffness and stability of (001) surface of the nanogranular c–s–h gel", Cem. Concr. Res. 102 (2017) 227–230.
[230] S.R. Hall, F.H. Allen, I.D. Brown, The crystallographic information file (cif): a new standard archive file for crystallography, Acta Crystallogr. A: Found. Crystallogr. 47 (1991) 655–685.
[231] T.N. Bhat, P. Bourne, Z. Feng, G. Gilliland, S. Jain, V. Ravichandran, B. Schneider, K. Schneider, N. Thanki, H. Weissig, J. Westbrook, H.M. Berman, The PDB data uniformity project, Nucleic Acids Res. 29 (2001) 214–218.
[232] H. Heinz, T.-J. Lin, R. Kishore Mishra, F.S. Emami, Thermodynamically consistent force fields for the assembly of inorganic, organic, and biological nanostructures: the interface force field, Langmuir 29 (2013) 1754–1765.
[233] S. Galmarini, A. Aimable, N. Ruffray, P. Bowen, Changes in portlandite morphology with solvent composition: atomistic simulations and experiment, Cem. Concr. Res. 41 (2011) 1330–1338.
[234] H. Tachikawa, K. Haga, S. Watanabe, K. Yamada, Local structures and electronic states of csh–sodium–h2o interface: nmr and dft studies, J. Phys. Chem. C 124 (2020) 5672–5680.
[235] I.-H. Svenum, I.G. Ringdalen, F.L. Bleken, J. Friis, D. Höche, O. Swang, Structure, hydration, and chloride ingress in c-s-h: insight from dft calculations, Cem. Concr. Res. 129 (2020), 105965.
[236] A.C. Van Duin, A. Strachan, S. Stewman, Q. Zhang, X. Xu, W.A. Goddard, Reaxffsio reactive force field for silicon and silicon oxide systems, J. Phys. Chem. A 107 (2003) 3803–3811.
[237] R.K. Mishra, A.K. Mohamed, D. Geissbühler, H. Manzano, T. Jamil, R. Shahsavari, A.G. Kalinichev, S. Galmarini, L. Tao, H. Heinz, et al., Cemff: a force field database for cementitious materials including validations, applications and opportunities, Cem. Concr. Res. 102 (2017) 68–89.
[238] K. Chenoweth, A.C. Van Duin, W.A. Goddard, Reaxff reactive force field for molecular dynamics simulations of hydrocarbon oxidation, J. Phys. Chem. A 112 (2008) 1040–1053.
[239] J.A. Lemkul, J. Huang, B. Roux, A.D. MacKerell, An empirical polarizable force field based on the classical drude oscillator model: development history and recent applications, Chem. Rev. 116 (2016) 4983–5013. PMID: 26815602.
[240] K. Kobayashi, H. Nakamura, A. Yamaguchi, M. Itakura, M. Machida, M. Okumura, Machine learning potentials for tobermorite minerals, Comput. Mater. Sci. 188 (2021), 110173.
[241] Y. Zhou, H. Zheng, W. Li, T. Ma, C. Miao, A deep learning potential applied in tobermorite phases and extended to calcium silicate hydrates, Cem. Concr. Res. 152 (2022), 106685.
[242] E.J. Maginn, R.A. Messerly, D.J. Carlson, D.R. Roe, J.R. Elliot, Best practices for computing transport properties 1. self-diffusivity and viscosity from equilibrium molecular dynamics [article v1. 0], Living J. Comput. Mol. Sci. 1 (2019), 6324–6324.
[243] A. Morandeau, M. Thiery, P. Dangla, Investigation of the carbonation mechanism of ch and csh in terms of kinetics, microstructure changes and moisture properties, Cem. Concr. Res. 56 (2014) 153–170.
[244] L. Liu, C. Sun, G. Geng, P. Feng, J. Li, R. Dähn, Influence of decalcification on structural and mechanical properties of synthetic calcium silicate hydrate (csh), Cem. Concr. Res. 123 (2019), 105793.
[245] J.J. Gaitero, I. Campillo, A. Guerrero, Reduction of the calcium leaching rate of cement paste by addition of silica nanoparticles, Cem. Concr. Res. 38 (2008) 1112–1118.
[246] Q. Zheng, J. Jiang, G. Xu, J. Yu, L. Tang, S. Li, New insights into the role of portlandite in the cement system: elastic anisotropy, thermal stability, and structural compatibility with c-s-h, Cryst. Growth Des. 20 (2020) 2477–2488.
[247] H. Manzano, A. Enyashin, J. Dolado, A. Ayuela, J. Frenzel, G. Seifert, Do cement nanotubes exist? Adv. Mater. 24 (2012) 3239–3245.
[248] C. Rodriguez-Navarro, A. Burgos-Cara, F.D. Lorenzo, E. Ruiz-Agudo, K. Elert, Nonclassical crystallization of calcium hydroxide via amorphous precursors and the role of additives, Cryst. Growth Des. 20 (2020) 4418–4432.
[249] M. Schönlein, J. Plank, A tem study on the very early crystallization of csh in the presence of polycarboxylate superplasticizers: transformation from initial csh globules to nanofoils, Cem. Concr. Res. 106 (2018) 33–39.
[250] N. Krautwurst, L. Nicoleau, M. Dietzsch, I. Lieberwirth, C. Labbez, A. Fernandez-Martinez, A.E. Van Driessche, B. Barton, S. Leukel, W. Tremel, Two-step nucleation process of calcium silicate hydrate, the nanobrick of cement, Chem. Mater. 30 (2018) 2895–2904.
[251] M. Fitzner, G.C. Sosso, S.J. Cox, A. Michaelides, The many faces of heterogeneous ice nucleation: interplay between surface morphology and hydrophobicity, J. Am. Chem. Soc. 137 (2015) 13658–13669. PMID: 26434775.
[252] G.C. Sosso, J. Chen, S.J. Cox, M. Fitzner, P. Pedevilla, A. Zen, A. Michaelides, Crystal nucleation in liquids: open questions and future challenges in molecular dynamics simulations, Chem. Rev. 116 (2016) 7078–7116. PMID: 27228560.
[253] A. Cuko, A. Macià, M. Calatayud, S.T. Bromley, Global optimisation of hydroxylated silica clusters: a cascade Monte Carlo basin hopping approach, Comput. Theor. Chem. 1102 (2017) 38–43.
[254] K. Yang, C.E. White, Modeling of aqueous species interaction energies prior to nucleation in cement-based gel systems, Cem. Concr. Res. 139 (2021), 106266.

Further reading

[164] M. Youssef, R.J.M. Pellenq, B. Yildiz, Glassy nature of water in an ultraconfining disordered material: the case of calcium-silicate-hydrate, J. Am. Chem. Soc. 133 (2011) 2499–2510.
[167] M.B.M. Pinson, E. Masoero, P.A.P. Bonnaud, H. Manzano, Q. Ji, S. Yip, J.J. J. Thomas, M.Z.M. Bazant, K.J.K. Van Vliet, H.M. Jennings, Hysteresis from multiscale porosity: modeling water sorption and shrinkage in cement paste, Phys. Rev. Appl. 3 (2015) 64009.
[168] L. Alarcon-Ruiz, G. Platret, E. Massieu, A. Ehrlacher, The use of thermal analysis in assessing the effect of temperature on a cement paste, Cem. Concr. Res. 35 (2005) 609–613.